Cu^{II} and Zn^{II} Coordination Chemistry of Pyrazole-Containing Polyamine Receptors − Influence of the Hydrocarbon Side Chain Length on the Metal Coordination

Carlos Miranda,[a] Francisco Escartí,[b] Laurent Lamarque,[a] Enrique García-España,*[b] Pilar Navarro,*[a] Julio Latorre,[b] Francisco Lloret,[b] Hermás R. Jiménez,[b] and María J. R. Yunta[c]

Dedicated to Prof. Dr. José Elguero

Keywords: Pyrazole macrocycles / Copper and zinc coordination / Acid-base and metal formation equilibria / Polyamine ligands / Paramagnetic NMR

The synthesis of a new macrocyclic receptor (**L⁴**) containing two 3,5-dimethylpyrazole units connected by dipropylenetriamine bridges is reported for the first time; pH-metric titrations indicate that **L⁴** shows six protonation steps in the pH range 2–11. In the absence of metal ions, the pyrazole moieties are not involved in acid-base processes in this pH range. Addition of Cu^{II} and Zn^{II} results in deprotonation of the pyrazole moieties which act as bis(monodentate) η^1:η^1 ligands. This induced deprotonation occurs at higher pH values than in the complexes of the analogous ligand containing diethylenetriamine bridges (**L¹**). The crystal structures of $[Cu_2(H_{-2}\mathbf{L^4})](ClO_4)_2$ and $[Zn_2(H_{-2}\mathbf{L^4})](ClO_4)_2$ obtained by treatment of $Na_2[H_{-2}\mathbf{L^4}]$ with either $Cu(ClO_4)_2{\cdot}6H_2O$ or $Zn(ClO_4)_2{\cdot}6H_2O$ in methanol followed by recrystallisation from water/methanol also show the deprotonation of the pyrazole moieties. The coordination geometry around each metal ion is square-pyramidal and involves all nitrogen atoms of the macrocycle. The crystal structure of $[Zn_2(H_{-2}\mathbf{L^1})](ClO_4)_2$ shows full involvement of all the nitrogen atoms of the macrocycle in the coordination to the metal ions. The coordination geometry can be defined as midway between a square pyramid and an irregular trigonal bipyramid. Treatment of neutral **L⁴** in methanol with $Cu(ClO_4)_2{\cdot}6H_2O$ yields a blue complex which, after heating in boiling water, crystallises as a red compound. Elemental microanalyses, ESI-MS and FAB-MS data of both forms of this complex are consistent with the formula $[Cu_2\mathbf{L^4}](ClO_4)_4{\cdot}2H_2O$. Furthermore, these data along with the paramagnetic ^1H NMR spectrum of the red form of the compound suggest a structure in which the pyrazole rings are deprotonated while the central nitrogen atoms of the bridging chains are protonated and consequently uncoordinated. The change from the blue (square-pyramidal) to the red form (square-planar) can be ascribed to dissociation of the water molecules which occupy the axial positions in the Cu^{II} coordination spheres of the blue form. The variation of the magnetic susceptibility of the red complex $[Cu_2\mathbf{L^4}](ClO_4)_4{\cdot}2H_2O$ and the complex $[Cu_2(H_{-2}\mathbf{L^4})](ClO_4)_2$ with temperature has been studied in the 2–300 K temperature range. Fitting of the experimental data provides J values which are among the highest found for doubly pyrazolate-bridged dicopper(II) complexes {J = −299 cm^{-1} for red-$[Cu_2\mathbf{L^4}](ClO_4)_4{\cdot}2H_2O$ and J = −286 cm^{-1} for $[Cu_2(H_{-2}\mathbf{L^4})](ClO_4)_2$}. A trinuclear Cu^{II} complex of formula $[Cu_3(H_{-2}\mathbf{L^4})](ClO_4)_4{\cdot}2MeOH$ was also isolated after treatment of **L⁴** with $Cu(ClO_4)_2{\cdot}6H_2O$ solutions of higher concentration.

[a] Instituto de Química Médica, Centro de Química Orgánica Manuel Lora Tamayo, CSIC,
c/ Juan de la Cierva 3, 28006 Madrid, Spain
E-mail: iqmnt38@iqm.csic.es
[b] Departamento de Química Inorgánica, Facultad de Química, Universidad de Valencia,
c/ Doctor Moliner 50, 46100 Burjassot (Valencia), Spain
Fax: (internat.) + 34-96-3864322
E-mail: enrique.garcia-es@uv.es
[c] Departamento de Química Orgánica, Facultad de Química, Universidad Complutense de Madrid,
Avda. Complutense s/n, 28040 Madrid, Spain
Supporting information for this article is available on the WWW under http://www.eurjic.org or from the author.

Introduction

Over the last decades a large amount of research effort has been devoted to identifying the biological roles of metal ions such as Cu^{II} and Zn^{II}. In order to achieve such a goal, different parallel approaches have been followed. The most straightforward consists of directly studying the active site in the metalloenzymes. A second approach, which has proved very useful in some instances,[1−3] has been to mimic the chemical features of the metal sites using smaller sized coordination compounds as models. The knowledge ob-

tained from the way in which metalloenzymes activate small molecules like H_2, N_2, CO_2, etc. has also resulted in considerable interest in the development of catalysts for industrial purposes.

A second biological aspect of metal complexes that has to be taken into account is their implications in pharmacology. For instance, complexes of macrocyclic ligands such as bicyclams and their Zn^{II} complexes have shown useful applications as potent anti-HIV-1 agents and several Mn^{II} and Cu^{II} complexes of hexaazamacrocycles have found applications as SOD mimics.[4] Another point of interest concerns the use of chelate ligands for selectively complexing and removing excess amounts of metal ions from which arise undesirable effects such as the oxidative damage detected in several neurodegenerative disorders.[5] An illustrative example comes from the use of the ligand PBT1 (clioquinol) for removing excess Cu^{II} which accumulates in the neocortex following the oxidative damage produced in Alzheimer disease.[6]

Therefore, the preparation and study of the coordination chemistry of ligands featuring new characteristics in their interaction with metal ions represents a challenge in coordination and biomedical chemistry. Ligands including 1*H*-pyrazole fragments offer a wealth of possibilities in this respect. The pyrazole unit can behave as a monodentate ligand through its sp^2 nitrogen atom or, upon deprotonation, as an $\eta^1{:}\eta^1$ bis(monodentate) bridging ligand (Scheme 1).[7,8]

Recently, we have examined the acid-base behaviour, Cu^{II} coordination chemistry and dopamine recognition capabilities of a series of pyrazole-containing polyamine macrocycles of different topologies [see ligands **1** (**L**^{1}) to **3** (**L**^{3}) in Scheme 2].[9−11] Here we extend these studies to the metal ion Zn^{II}. Additionally, we report on the synthesis of the pyrazole-containing macrocycle 3,7,11,14,15,18,22,26,29,30-decaazatricyclo[26.2.1.1^{13,16}]dotriacontane-1(31),13,16(32),28-tetraene (**4**) (**L**^{4}) (see Scheme 2) which has only propylenic chains and the preparation of its disodium dipyrazolate salt **4′** [$Na_2(H_{-2}$**L**^{4})]. We discuss the effect of the propylenic chains on the acid-base behaviour and on the Cu^{II} and Zn^{II} coordination chemistry in aqueous solution. We also report different Cu^{II} and Zn^{II} complexes prepared either from **4** and **4′** or from the ligands **1**−**3** and we discuss the influence of the hydrocarbon chain length on the coordination features of these new complexes.

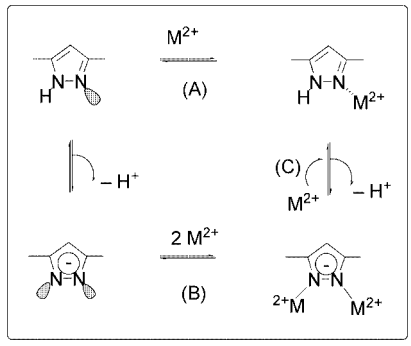

Scheme 1

Results and Discussion

Synthesis of 4 and 4′

The preparation of **4** was performed by a [2+2] dipodal condensation of 3,5-pyrazoledicarbaldehyde with *N*-(3-aminopropyl)-1,3-propanediamine in methanol at room temperature, followed by in situ reduction of the resultant Schiff base with $NaBH_4$. After careful purification firstly by chromatography and then by crystallisation from toluene, **4** (**L**^{4}) was isolated as a pure solid of melting point 154−156 °C in 49% yield. Compound **4** and its hydrochloride **4**·6HCl

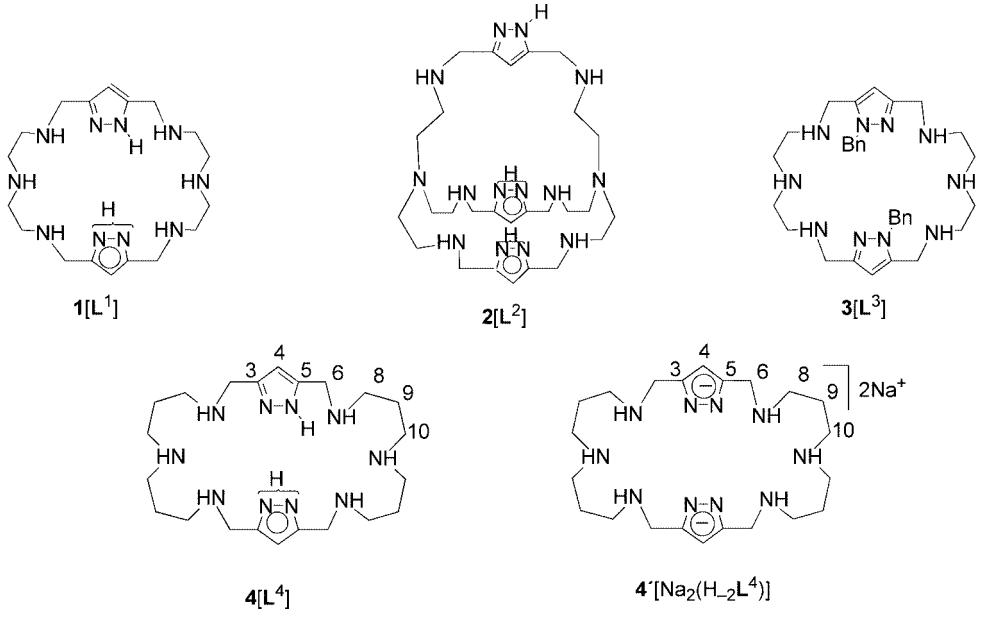

Scheme 2

Table 1. Comparison of ^1H and ^{13}C NMR spectroscopic data (δ [ppm], D_2O) of **4** recorded at pH = 10.5 and 8.0 and **4**·6HCl recorded at pH = 3.7

	4 (1) pH = 10.5	**4** (2) pH = 8.0	**4**·6HCl (3) pH = 3.7	Δδ (2−1)	Δδ (3−2)
4-H	6.07 (s, 2 H)	6.22 (s, 2 H)	6.63 (s, 2 H)	0.15	0.41
6-H	3.53 (s, 8 H)	3.71 (s, 8 H)	4.26 (s, 8 H)	0.18	0.55
8-H	2.26 (t. 8 H)[a]	2.61 (t, 8 H)[a]	3.05 (m, 8 H)	0.35	0.44
9-H	1.37 (m, 8 H)	1.70 (m, 8 H)	2.01 (m, 8 H)	0.33	0.31
10-H	2.26 (t. 8 H)[a]	2.87 (t, 8 H)[a]	3.05 (m, 8 H)	0.61	0.18
	4 (1) pH = 10.5	**4** (2) pH = 8.0	**4**·6HCl (3) pH = 3.7	Δδ (2−1)	Δδ (3−2)
C-3,5	147.71	145.40[b]	139.20	−2.31	−6.20
C-4	103.68	104.52	109.01	0.84	4.58
C-6	43.79	43.64	42.68	−0.15	−0.96
C-8	45.34	45.26	43.83	−0.08	−1.43
C-9	28.40	24.79	22.81	−3.61	−1.98
C-10	46.55	45.96	44.65	−0.59	−1.31

[a] J = 7 Hz. [b] Broad signal.

(m.p. 265−268 °C) have been fully characterised by elemental analyses and NMR spectroscopy.

Table 1 shows a comparison of the ^1H and ^{13}C NMR spectroscopic data of the new ligand **4**, recorded in D_2O at pH = 10.5 and 8.0, with those of its hexahydrochloride **4**·6HCl recorded at pH = 3.7. The signals have been analysed on the basis of their HMQC and multiple-bond HMBC 2D NMR heteronuclear correlation spectra. The above ^1H NMR spectra are graphically compared in the Supporting Information [Figure 1S (A−C)] (for Supporting Information see also the footnote on the first page of this article).

As usually occurs for 3,5-disubstituted 1*H*-pyrazole derivatives, at pH = 10.5 (where the nonprotonated species predominates) **4** shows a very simple pattern of signals which indicates that because of the fast prototropic equilibrium of the pyrazole ring, the compound exhibits an average fourfold symmetry on the NMR time scale. The carbon atoms labelled C-3 and C-5 (for the labelling see Scheme 2) appear together as a sharp signal and the pairs of methylene carbon atoms C-6, C-8, C-9 and C-10 are magnetically equivalent.

In general, the pH-dependent variation of the NMR resonances of the β-carbon atoms and of the hydrogen atoms bound to the α-carbon atoms with respect to the protonated nitrogen atoms are of great help in establishing protonation sequences of polyamine molecules.[9] As can be derived from the basicity constants, the two first protonations of $\mathbf{L^4}$ occur in the pH range of 11−8. Thus, in the NMR spectra of **4** recorded at pH = 8.0 (Table 1), the carbon signal shifted the most upfield is that of carbon atoms C-9 ($\Delta\delta$ = −3.61 ppm), whereas the signal of carbon atoms C-8 and that of the quaternary carbon atoms C-3,5 do not experience significant shifts in this pH region. In the same way, the most downfield shifted ^1H signal is that of 10-H ($\Delta\delta$ = 0.61 ppm), clearly indicating that **4** is protonated firstly at the centre nitrogen atoms of the bridging chains. On the other hand, by comparing the NMR signals of **4** at pH = 8 and those of **4**·6HCl at pH = 3.7 (Table 1) it can be observed that after protonation of the aliphatic nitrogen atoms closer to the pyrazole rings, the most downfield shifted hydrogen signals are those of 6-H and 8-H ($\Delta\delta$ = 0.55 and 0.44 ppm, respectively) and that the signals of the methylene carbon atoms which experience the largest upfield variations are C-9 = −1.98 ppm) which are located in the β-position with respect to the above-mentioned nitrogen atoms.

Furthermore, in **4**·6HCl, the signals of the pyrazole carbon atoms C-3,5 and C-4 (located in the β- and γ-positions, respectively, in relation to the closer protonated aliphatic nitrogen atoms) also experience large upfield ($\Delta\delta$ = 6.20 ppm for C-3,5) and downfield ($\Delta\delta$ = 4.58 ppm for C-4) shifts. These variations are of a similar order to those previously reported for $\mathbf{L^1}$.[9] It is important to point out that such variations do not reflect any particular implication of the pyrazole subunits in the protonation process, since it is well known that β- and γ-aromatic carbon atoms belonging to polyamine-bridged cyclophanes containing benzene units also bear similar chemical shifts upon protonation.[12,13] Finally, we also obtained the disodium dipyrazolate salt **4′** [$Na_2(H_{-2}\mathbf{L^4})$] as a pure solid (m.p. 208−210 °C) in 98% yield, by heating the free ligand **4** to reflux with 2 equiv. of NaOH in MeOH.

Acid-Base Behaviour

Table 2 includes the stepwise protonation constants of the new receptor $\mathbf{L^4}$ and those previously reported for compounds **1** ($\mathbf{L^1}$) to **3** ($\mathbf{L^3}$).[9−11] The basicity constants of **4** ($\mathbf{L^4}$), with only propylenic chains are higher than those of $\mathbf{L^1}$ containing only ethylenic chains and are also higher than those of the compound with ethylenic chains and *N*-benzylpyrazole spacers ($\mathbf{L^3}$). The differences between the stepwise constants of $\mathbf{L^4}$ and those of $\mathbf{L^1}$ and $\mathbf{L^3}$ are particularly large for the fifth and sixth protonation steps (Table 2). The fifth and six protonations occur at the central nitrogen atoms of the polyamine chains of the macrocycle. Therefore, at this stage, the incoming proton will notice a lower elec-

Table 2. Protonation constants of the receptors **L¹** to **L⁴** determined in 0.15 mol·dm^{-3} NaCl at 298.1 K

Reaction[a]	**L¹** [b]	**L²** [c]	**L³** [b]	**L⁴** [d]
H + **L** = H**L**	9.74	9.54	8.90	10.05(2)[e]
H + H**L** = H_2**L**	8.86	8.71	8.27	9.34 (2)
H + H_2**L** = H_3**L**	7.96	7.72	6.62	7.63 (3)
H + H_3**L** = H_4**L**	6.83	6.55	5.85	7.07 (3)
H + H_4**L** = H_5**L**	4.57	6.52	3.37	6.45 (3)
H + H_5**L** = H_6**L**	3.19	5.22	2.27	5.55 (4)
log β[f]	41.1	44.3	35.3	46.1

[a] Charges omitted for clarity. [b] Taken from ref.[9] [c] Taken from ref.[11] [d] This work. [e] Values in parentheses are standard deviations in the last significant figure. [f] log $\beta = \Sigma \log K_{HjL}$.

trostatic repulsion from the adjacent polyammonium sites in **L⁴** than in **L¹** or in **L³** due to the presence of the larger propylenic chains.[14] Curiously, the basicities displayed by **L⁴** and the cryptand **L²** are rather similar even if their structures and numbers of nitrogen atoms are different.

The high degree of protonation that **L⁴** presents at physiological pH values (mean number of protons at pH = 7.4 is 3.02) makes this receptor a promising candidate for the coordination of anionic or polar species.

Metal Coordination in Aqueous Solution

The stability constants for the formation of Cu^{II} complexes of **4** (**L⁴**) together with those previously reported for the related receptors **1** (**L¹**) to **3** (**L³**) under the same experimental conditions are shown in Table 3.[11] The stability constants for the interaction of Zn^{II} with **L¹** to **L⁴** determined in this work are presented in Table 4.

With Cu^{II}, **L⁴** forms mononuclear $[Cu(H_xL)]^{(x+2)}$ complexes with $x = 0$, 1, 2 and 3 and dinuclear $[Cu_2(H_xL)]^{(x+4)}$ species with $x = -1$, -2 and -3. The extent of formation of each one of these complexes depends on pH, M/L molar ratio and concentration as can be seen in Figure 1 which shows the distribution diagrams for the Cu^{II} complexes of **L⁴** in molar ratios of 1:1 (Figure 1, A) and 2:1 (Figure 1, B), complexes of **L¹** in a molar ratio of 2:1 (Figure 1, C) and for the Zn^{II} complexes of **L⁴** and **L¹** in a molar ratio 2:1 (Figure 1, D and E, respectively).

The stability constant for the species $[Cu\mathbf{L^4}]^{2+}$ is intermediate between that found for $[Cu\mathbf{L^1}]^{2+}$ (**L¹** is the analogous macrocycle with ethylenic chains) and that of $[Cu\mathbf{L^3}]^{2+}$ (**L³** being the compound with ethylenic chains and *N*-benzylated pyrazole spacers) (Entry 4 in Table 3). The same situation occurs for the dinuclear $[Cu_2\mathbf{L}]^{4+}$ complexes (Entry 7). The sequence of five-membered chelate rings present in **L¹** leads to a stronger coordination to Cu^{II} than the sequence of six-membered rings present in **L⁴**. The situation for **L³** is different since the substituted spacers cannot be deprotonated and each one provides only an sp^2 nitrogen donor over all the pH ranges studied.

Deprotonation of the pyrazole spacers induced by coordination to metal ions is a characteristic feature of this heterocycle.[8,11,15–17] The structure of **L⁴** enables an analysis of the influence of the length of the hydrocarbon chain and thereby of the denticity of the chelate rings on such deprotonation processes. The distribution diagrams calculated for an M/L ratio of 2:1 shown in Figure 1 indicate that while the species $[Cu_2(H_{-2}L)]^{2+}$ with both pyrazole moieties deprotonated is already predominant in solution at pH ≈ 4.3 for **L¹**, a similar species is produced only at pH

Table 3. Stability constants for the formation of Cu^{II} complexes of the receptors **L¹**, **L²**, **L³** and **L⁴** determined in 0.15 mol·dm^{-3} NaCl at 298.1 K

Entry	Reaction[a]	**L¹** [b]	**L²** [b]	**L³** [b]	**L⁴** [c]
1	Cu + L + 3 H = CuH_3L				37.68(9)
2	Cu + L + 2 H = CuH_2L	35.05(2)[d]	35.42(8)	27.9(1)	32.64(6)
3	Cu + L + H = CuHL	30.82(2)	28.85(7)	22.12(8)	25.91(4)
4	Cu + L = CuL	23.48(3)	21.76(6)	13.60(7)	17.83(8)
5	Cu + L = $CuH_{-1}L$ + H		13.05(3)		
6	2 Cu + L + H = Cu_2HL		39.04(7)	29.37(5)	
7	2 Cu + L = Cu_2L	34.45(3)	36.72(3)	26.27(3)	28.72(2)
8	2 Cu + L = $Cu_2H_{-1}L$ + H		31.31(5)	16.85(4)	23.62(3)
9	2 Cu + L = $Cu_2H_{-2}L$ + 2 H	26.56(3)	24.13(5)	7.06(3)	15.69(8)
10	2 Cu + L = $Cu_2H_{-3}L$ + 3 H				5.87(7)
11	CuH_2L + H = CuH_3L				5.04
12	CuHL + H = CuH_2L	4.23	6.57	5.78	6.73
13	CuL + H = CuHL		7.09	8.52	8.08
14	CuL = $CuH_{-1}L$ + H	7.34	8.71		
15	CuL+Cu = Cu_2L	10.97	12.67		10.89
16	Cu_2L + H = Cu_2HL		2.32	3.1	
17	Cu_2L = $Cu_2H_{-1}L$ + H		−5.41	−9.42	−5.1
18	$Cu_2H_{-1}L$ = $Cu_2H_{-2}L$ + H		−7.18	−9.79	−8.07
19	Cu_2L = $Cu_2H_{-2}L$ + 2 H	−7.89	−12.59	−19.21	−13.03
20	$Cu_2H_{-2}L$ = $Cu_2H_{-3}L$ + H				−9.72

[a] Charges omitted for clarity. [b] Taken from ref.[11] [c] This work. [d] Values in parentheses are standard deviations in the last significant figure.

Table 4. Stability constants for the formation of Zn^{II} complexes of the receptors **L¹**, **L²**, **L³** and **L⁴** determined in 0.15 mol·dm^{-3} NaCl at 298.1 K

Entry	Reaction[a]	**L¹**	**L²**	**L³**	**L⁴**
1	$Zn + L + 3\,H = ZnH_3L$	32.26(7)[b]	32.72(2)		
2	$Zn + L + 2\,H = ZnH_2L$	26.4(2)	27.42(3)		
3	$Zn + L + H = ZnHL$	22.26(4)	22.227(9)	16.67(2)	17.54(3)
4	$Zn + L = ZnL$	15.74(4)	14.12(2)	8.53(4)	8.8(1)
5	$Zn + L = ZnH_{-1}L + H$	7.21(4)	3.91(2)	−0.43(4)	−1.0(1)
6	$2\,Zn + L + H = Zn_2HL$				
7	$2\,Zn + L = Zn_2L$		20.19(3)	14.40(2)	14.42(3)
8	$2\,Zn + L = Zn_2H_{-1}L + H$	14.63(5)	14.71(1)	6.04(4)	8.22(1)
9	$2\,Zn + L = Zn_2H_{-2}L + 2\,H$	8.94(4)	4.75(2)	−2.71(3)	−1.50(3)
10	$2\,Zn + L = Zn_2H_{-3}L + 3\,H$			−12.81(3)	
11	$3\,Zn + L = Zn_3H_{-3}L + 3\,H$		1.80(4)		
12	$ZnH_2L + H = ZnH_3L$	5.9	5.30		
13	$ZnHL + H = ZnH_2L$	4.1	5.19		
14	$ZnL + H = ZnHL$	6.52	8.11	8.14	8.7
15	$ZnL = ZnH_{-1}L + H$	−8.53	−10.21	−8.96	−9.8
16	$ZnL + Zn = Zn_2L$		6.07	5.87	5.62
17	$Zn_2L + H = Zn_2HL$				
18	$Zn_2L = Zn_2H_{-1}L + H$		−5.48	−8.36	−6.2
19	$Zn_2H\text{-}_1L = Zn_2H_{-2}L + H$	−5.69	−9.96	−8.75	−9.72
20	$Zn_2L = Zn_2H_{-2}L + 2\,H$		−15.44	−17.11	−15.92
21	$Zn_2H_{-2}L = Zn_2H_{-3}L + H$				

[a] Charges omitted for clarity. [b] Values in parentheses are standard deviations in the last significant figure.

> 8 for **L⁴** (Figure 1, B). The first average deprotonation of $[Cu_2\mathbf{L^4}]^{2+}$ gives $pK_{a1} = 5.1$ and the second one $pK_{a2} = 8.1$.

However, care has to be taken in drawing such a conclusion since in the red solid red-$[Cu_2\mathbf{L^4}](ClO_4)_4\cdot 2H_2O$ {red-[**13**]$(ClO_4)_4\cdot 2H_2O$}, prepared from neutral **L⁴** and $Cu(ClO_4)_2\cdot 6H_2O$ (vide infra), the two pyrazole units are deprotonated while the central amino groups of both chains are protonated giving the ligand an overall charge of zero (see **13** in Scheme 3). Therefore, Cu^{II} coordination induces the ready deprotonation of the pyrazole nitrogen atoms which, in this complex, occurs at a lower pH than the deprotonation of the central propylenic chain. This is a particular feature of **L⁴** not observed in the related ligand **L¹** with ethylenic chains. The higher basicity of **L⁴** in its two first protonation steps should facilitate this situation. Such behaviour contrasts with that of the free ligands, for which neither deprotonation nor protonation processes occur at the pyrazole rings throughout the pH range of 2−11.[9,11] On the other hand, all the dinuclear Cu^{II} complexes are EPR-silent.

The stability constants gathered in Table 4 show that, as expected, the Zn^{II} complexes display remarkably lower stabilities than the Cu^{II} analogues (see for instance, Entries 4 in Table 3 and 4 for the $[M\mathbf{L}]^{2+}$ complexes). In all the Zn/L systems, formation of mono- and dinuclear complexes can be observed and for the Zn/**L²** system even a trinuclear species $[Zn_3(H_{-3}\mathbf{L^2})]^{4+}$ was detected. The degree of protonation of the mononuclear complexes reaches a value of 3 for **L¹** and **L²** {$[Zn(H_3\mathbf{L})]^{5+}$ species} and only of 1 for the systems Zn/**L³** and Zn/**L⁴** {i.e. $[Zn(H\mathbf{L})]^{3+}$ species}. The degree of protonation of the dinuclear Zn^{II} complexes varies between 0 and −3. In the case of the Zn/**L¹** system, it has not been possible to identify any nondeprotonated dinuclear species (see distribution diagram in Figure 1). A comparison with Cu^{II} shows that for Zn^{II}, the deprotonation of pyrazole is shifted approximately two units to higher pH values as a result of the poorer inductive effect exerted by this metal ion. Taking into account the crystal structure of $[Zn_2(H_{-2}\mathbf{L^4})](ClO_4)_2$ and the spectroscopic data (vide infra) it is likely, that in the two species $[Zn_2(H_{-1}\mathbf{L^4})]^{3+}$ and $[Zn_2(H_{-2}\mathbf{L^4})]^{2+}$, both pyrazole groups are deprotonated. In $[Zn_2(H_{-1}\mathbf{L^4})]^{3+}$ one of the central nitrogen atoms of the bridging chain will be protonated. In the case of **L¹** the species $[Zn_2(H_{-1}\mathbf{L^1})]^{3+}$ cannot be detected and the only dinuclear species found in solution is $[Zn_2(H_{-2}\mathbf{L^1})]^{2+}$ (Figure 1, D and E). For the cryptand **L²** the situation is analogous to that of **L¹** and the species $[Zn_2(H_{-1}\mathbf{L^2})]^{3+}$ can be postulated as having the two pyrazole moieties involved in coordination to Zn^{II} being deprotonated, while the pyrazole in the noncoordinating bridge will be nondeprotonated and one of the amino groups in this region will be protonated. Such a situation has already been observed in the crystal structure of the analogous Cu^{II} complex of **L²**.[11] Finally, in the ligand with *N*-benzylated pyrazole spacers, the main species in solution at neutral pH, is $[Zn_2\mathbf{L^3}]^{4+}$. Deprotonation of the coordinated water molecules to give hydroxo species requires higher pH values.

Synthesis of Solid Zn^{II} Dinuclear Complexes from Polyamine Receptors with Ethylenic Chains 1 (L¹) to 3 (L³)

Some time ago the in situ deprotonation of ligands **1** (**L¹**) and **2** (**L²**) upon addition of NaOH, as well as the formation of Zn^{II} pyrazolate complexes was observed using NMR techniques in $[D_6]DMSO/D_2O$ mixtures.[18,19] However,

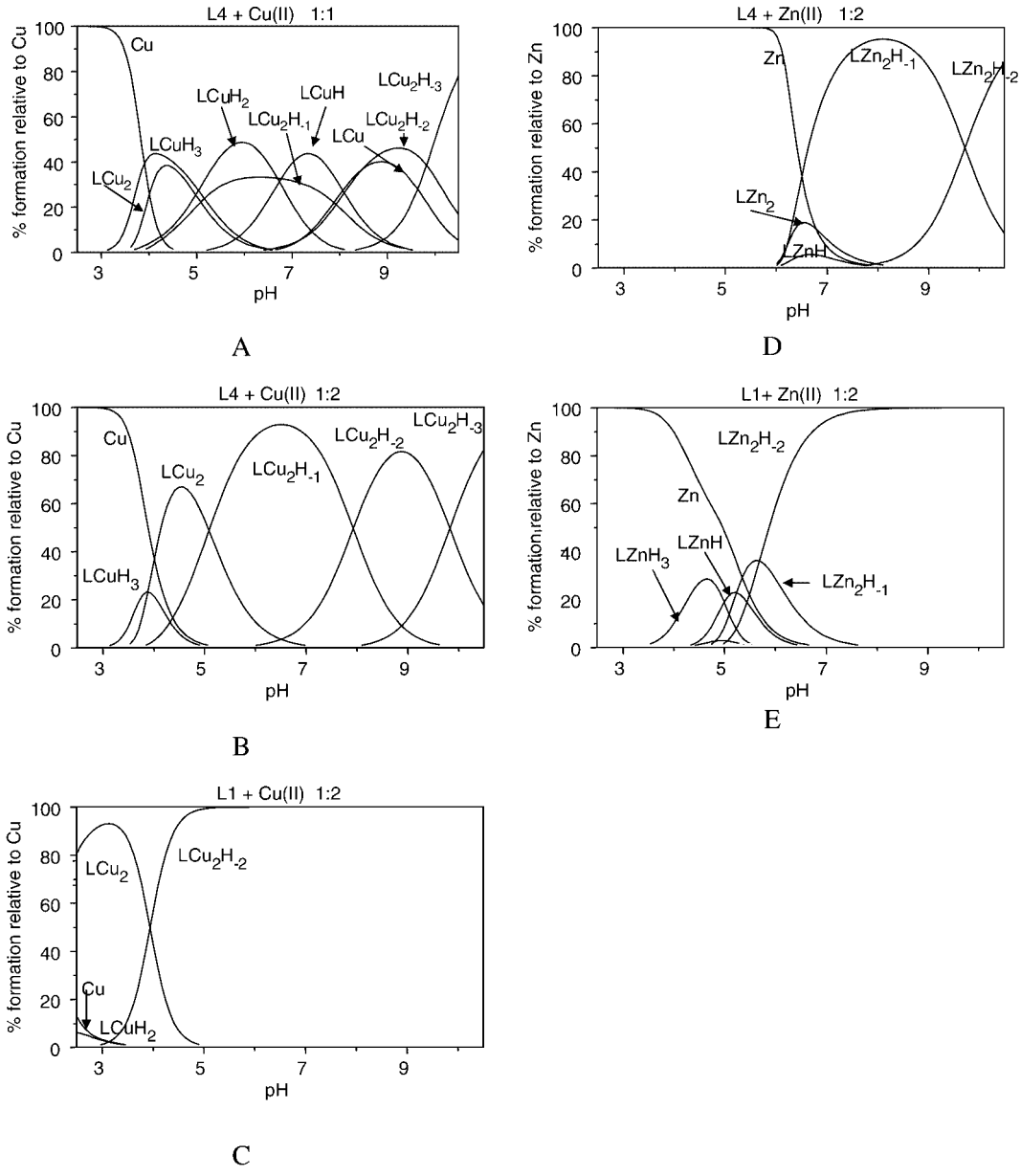

Figure 1. Distribution diagrams for the species existing in equilibrium in the systems: A) $Cu^{II}/\mathbf{L^4}$ molar ratio 1:1, B) $Cu^{II}/\mathbf{L^4}$ molar ratio 2:1, C) $Cu^{II}/\mathbf{L^1}$ molar ratio 2:1, D) $Zn^{II}/\mathbf{L^4}$ molar ratio 2:1, E) $Zn^{II}/\mathbf{L^1}$ molar ratio 2:1; the concentration of ligand is 1×10^{-3} M in all systems

none of the latter mentioned complexes were either isolated or structurally characterised as solid compounds. However, by treating the neutral ligands $\mathbf{L^1}$ to $\mathbf{L^3}$ with $Zn(ClO_4)_2 \cdot 6H_2O$ in methanol (molar ratio M/L = 2:1) we have now isolated three new solid complexes which were recrystallised from water. The analytical and MS data of these compounds are consistent with the formulae $[Zn_2(H_{-2}\mathbf{L^1})](ClO_4)_2$ $\{[\mathbf{8}](ClO_4)_2\}$, $[Zn_2(H_{-2}\mathbf{L^2})](ClO_4)_2 \cdot 4H_2O$ $\{[\mathbf{9}](ClO_4)_2 \cdot 4H_2O\}$ and $[Zn_2\mathbf{L^3}](ClO_4)_4 \cdot 6H_2O$ $\{[\mathbf{10}](ClO_4)_4 \cdot 6H_2O\}$ (Scheme 3). Electrospray ionisation (ESI-MS) and fast atom bombardment (FAB-MS) mass spectrometry have been used for the characterisation of all the new Zn^{II} complexes.[20] Besides, in the case of $[\mathbf{8}](ClO_4)_2$, suitable crystals for X-ray analysis were grown from the aqueous solution (vide infra).

The above data support the fact that in the case of $\mathbf{L^1}$ and $\mathbf{L^2}$, Zn^{II} coordination induces the deprotonation of the pyrazole rings to afford the pyrazolate bridging ligand without the need to add a base. On the other hand, considering that the structure of the starting ligand $\mathbf{L^3}$ corresponds to a constitutional isomer in which the 1-benzylpyrazole substituents are in positions opposite each other displaying C_2 symmetry[9] and taking into account the crystal structure of the analogous Cu^{II} complex $[\mathbf{7}](ClO_4)_4 \cdot 4H_2O$,[11] it is reasonable to assume that in the Zn^{II} complex $[\mathbf{10}](ClO_4)_4 \cdot 6H_2O$ the sp^2 nitrogen atoms of the pyrazole rings are also involved in the coordination to the metal ions.

The ESI (positive mode) and FAB mass spectra of complex $\{[\mathbf{8}] \cdot (ClO_4)_2\}$ show common peaks at m/z (%) = 615.1 (10) and 615.4 (10), respectively, which confirm the presence

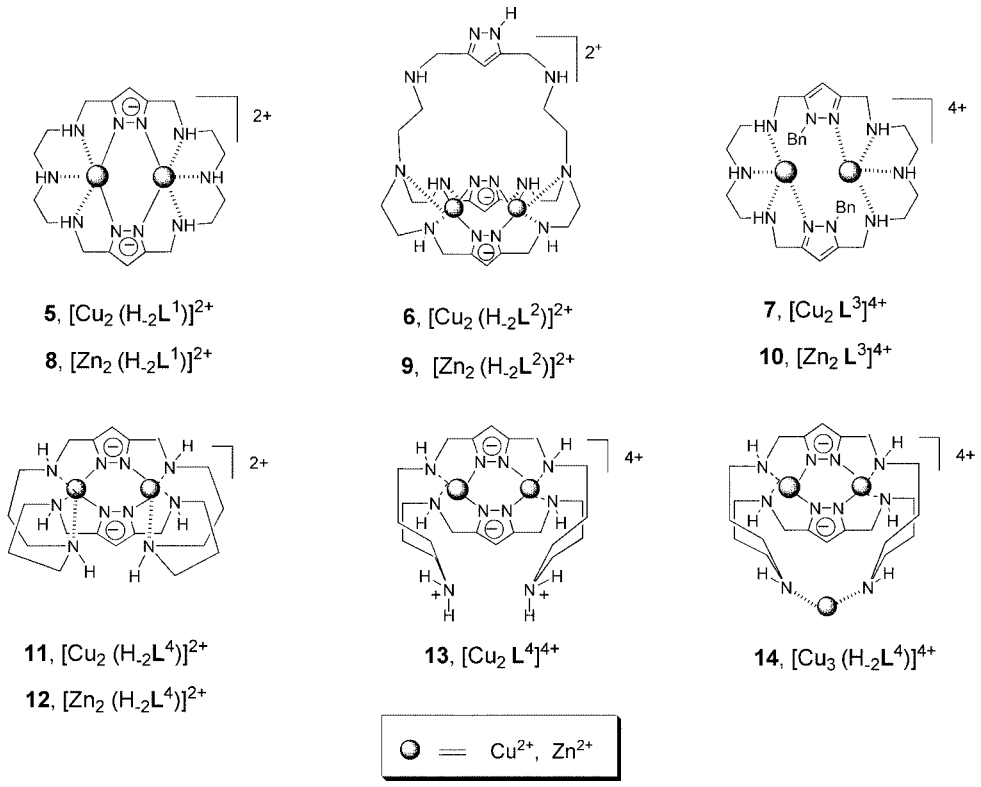

Scheme 3

of the dinuclear $[Zn_2(H_{-2}\mathbf{L^1})(ClO_4)]^+$ species, as well as intense peaks at *m*/*z* (%) = 453.4 (100) and 453.2 (47), respectively, corresponding to the species $[Zn(H_{-1}\mathbf{L^1})]^+$ generated by loss of $Zn(ClO_4)_2$.

Similarly, in both the ESI and FAB mass spectra of $[\mathbf{9}](ClO_4)_2{\cdot}4H_2O$, the protonated molecular ion $[Zn_2(H_{-2}\mathbf{L^2})(ClO_4)_2]H^+$ appears at *m*/*z* (%) = 893.2 (2) and 893.1 (23), respectively, and the ionic species $[Zn_2(H_{-2}\mathbf{L^2})(ClO_4)]^+$ is confirmed by the presence of intense peaks at *m*/*z* (%) = 793.2 (73) and 793.3 (63), respectively.

Finally, in the ESI (positive mode) and the FAB mass spectra of complex $[Zn_2\mathbf{L^3}](ClO_4)_4{\cdot}6H_2O$ appear common peaks which clearly support the proposed structure. At *m*/*z* (%) = 995.1 (5 and 44, respectively) appears a peak corresponding to the dinuclear $[Zn_2\mathbf{L^3}(ClO_4)_3]^+$ species formed from the molecular ion by loss of perchlorate and at *m*/*z* (%) = 733.5 (54) and 733.3 (23), respectively, a peak attributable to the ionic species $[Zn\mathbf{L^3}(ClO_4)]^+$ formed by successive loss of $Zn(ClO_4)_2$ and ClO_4^- can be observed.

Crystal Structure of $[Zn_2(H_{-2}L^1)](ClO_4)_2$ {[8](ClO4)2}

Crystals of $[Zn_2(H_{-2}\mathbf{L^1})](ClO_4)_2$ suitable for X-ray analysis were obtained by concentrating aqueous solutions containing $\mathbf{L^1}$ and $Zn(ClO_4)_2$ at pH = 9. The structure consists of $[Zn_2(H_{-2}\mathbf{L^1})]^{2+}$ cations and perchlorate anions. Each Zn^{II} is coordinated by the three nitrogen atoms from one of the polyamine bridges and by one sp^2 nitrogen atom from each one of the pyrazole units which are deprotonated

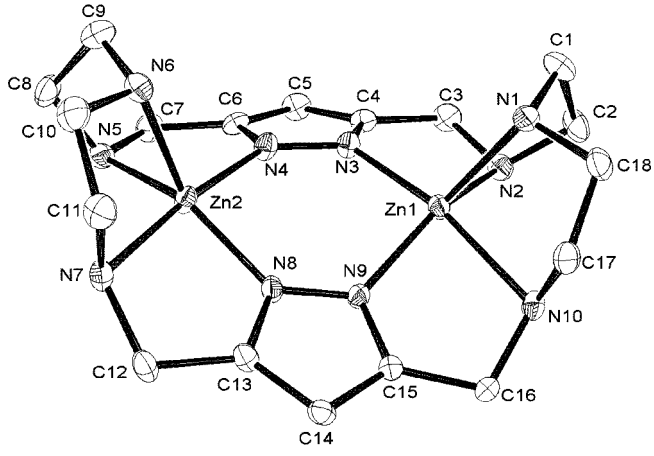

Figure 2. ORTEP drawing for the cation $[Zn_2(H_{-2}\mathbf{L^1})]^{2+}$ (**8**); thermal ellipsoids are drawn at the 30% probability level

and behave as bridging $\eta^1{:}\eta^1$-bis(monodentate) pyrazolate ligands (see Figure 2). The coordination geometry around each one of the metal ions can be defined as midway between a strongly distorted square pyramid and a trigonal bipyramid. The percentage of trigonal-bipyramidal units calculated by means of the facial planes[21] is 44.5% for the Zn1 site and 50.7% for the Zn2 site.

The shorter distances in the coordination spheres of both metal ions are those involving the pyrazolate sp^2 nitrogen atoms (see Table 5) and the largest ones are those of the amino groups adjacent to the pyrazole fragments. In order

to achieve such a coordination geometry the central part of the chains are forced to move in the same direction giving something of a boat-like shape (Figure 2).

Table 5. Selected bonds lengths [Å] and angles [°] of [**8**]$(ClO_4)_2$

Parameter	Length/angle
Zn1−N1	2.110(5)
Zn1−N2	2.212(5)
Zn1−N3	2.037(4)
Zn1−N9	2.027(4)
Zn1−N10	2.267(5)
Zn2−N4	2.027(4)
Zn2−N5	2.181(5)
Zn2−N6	2.109(5)
Zn2−N7	2.235(5)
Zn2−N8	2.005(4)
N1−Zn1−N2	83.3(2)
N1−Zn1−N3	110.4(2)
N1−Zn1−N9	128.7(2)
N1−Zn1−N10	81.1(2)
N2−Zn1−N3	78.3(2)
N2−Zn1−N10	103.9(2)
N3−Zn1−N9	95.4(2)
N9−Zn1−N10	76.6(2)
N4−Zn2−N5	79.5(2)
N4−Zn2−N6	101.6(2)
N4−Zn2−N8	94.9(2)
N5−Zn2−N6	83.8(2)
N5−Zn2−N7	106.8(2)
N6−Zn2−N7	82.0(2)
N6−Zn2−N8	125.2(2)
N7−Zn1−N8	78.3(2)

The Zn−Zn distance (3.99 Å) is close to those found for the analogous Cu^{II} complexes of $\mathbf{L^1}$ and $\mathbf{L^2}$, implying that the rigidity of the pyrazole spacer is the main factor controlling this parameter. It is interesting to remark that, as already observed in the systems Cu/$\mathbf{L^1}$ and Cu/$\mathbf{L^2}$,[11,17] Cu^{II} coordination causes the ready deprotonation of the pyrazole moieties without requiring any addition of base.

Synthesis of Cu^{II} and/or Zn^{II} Dipyrazolate Complexes $[Cu_2(H_{-2}L^4)](ClO_4)_2$ {[**11**]$(ClO_4)_2$} and $[Zn_2(H_{-2}L^4)](ClO_4)_2$ {[**12**]$(ClO_4)_2$} from **4′**

Synthesis and Spectroscopic Characterisation

In order to unequivocally obtain Cu^{II} and Zn^{II} dipyrazolate complexes we first used the disodium dipyrazolate salt **4′** (Scheme 2) as a starting material. Treatment of **4′** with $Cu(ClO_4)_2{\cdot}6H_2O$ (2 equiv.) in MeOH afforded a blue solid which, after being crystallized from a 2:3 water/MeOH mixture, gave the Cu^{II} dipyrazolate complex $[Cu_2(H_{-2}L^4)](ClO_4)_2$ {[**11**]$(ClO_4)_2$}.

The ESI (positive mode) mass spectrum of [**11**]$(ClO_4)_2$ in MeOH shows two intense peaks at *m*/*z* (%) = 671.0 (100) and 571.2 (58) which are assignable to the molecular species $[Cu_2(H_{-2}L^4)(ClO_4)]^+$ and $[Cu_2(H_{-3}L^4)]^+$, respectively. These confirm that the compound is a dinuclear Cu^{II} dipyrazolate complex. There also appears a fairly weak peak at *m*/*z* = 508.1 corresponding to the mononuclear $[Cu(H_{-1}L^4)]^+$ species which may be formed from the monoprotonated molecular ion $[Cu_2(H_{-1}L^4)(ClO_4)_2]^+$ by loss of $Cu(ClO_4)_2$.

The Zn^{II} dinuclear complex $[Zn_2(H_{-2}L^4)](ClO_4)_2$ {[**12**]$(ClO_4)_2$} (Scheme 3) was obtained by treatment of the sodium salt **4′** with 2 equiv. of $Zn(ClO_4)_2{\cdot}6H_2O$ according to a similar procedure to that previously mentioned. After crystallisation from a water/methanol mixture, the analytical and spectroscopic data of the white solid obtained were consistent with formula $[Zn_2(H_{-2}L^4)](ClO_4)_2$ {[**12**]$(ClO_4)_2$}. In its ESI (positive mode) mass spectrum, three main peaks detected at *m*/*z* (%) = 671.2 (32), 609.3 (27) and 509.4 (100) are attributable to the ionic species $[Zn_2(H_{-2}L^4)ClO_4]^+$, $[Zn(L^4)ClO_4]^+$ and $[Zn(H_{-1}L^4)]^+$, respectively.

The structure of $[Zn_2(H_{-2}L^4)](ClO_4)_2$ {[**12**]$(ClO_4)_2$} in solution was also fully characterised by NMR spectroscopy. In Tables 6 and 7 are gathered the respective ^1H and ^{13}C NMR spectroscopic data of this compound recorded in [D_6]DMSO together with those of the dipyrazolate salt **4′** and those of the free ligand **4**. Table 6 verifies that the ^1H NMR spectroscopic data of **4** and **4′** are similar. Each shows a single set of signals for all the methylene protons, the chemical shift differences between **4** and **4′** being lower than 0.2 ppm. However, in the ^1H NMR spectrum of $[Zn_2(H_{-2}L^4)]^{2+}$ (**12**) (Figure 3, A), the methylene protons 6-H_2, 8-H_2 and 9-H_2 which are neighbours of the pyrazole

Table 6. Comparison of the ^1H NMR spectra (δ [ppm], [D_6]DMSO) of the free ligand **4**, its sodium dipyrazolate salt **4′** and the Zn^{II} dipyrazolate complex [**12**]$(ClO_4)_2$

	4	**4′**	[**12**]$(ClO_4)_2$
4-H	5.99 (s, 2 H)	5.82 (s, 2 H)	5.77 (s, 2 H)
6-H_A	3.56 (s, 4 H)	3.56 (s, 4 H)	4.02 (dd, 4 H)[a]
6-H_B	3.56 (s, 4 H)	3.56 (s, 4 H)	3.50 (dd, 4 H)[b]
8-H_A	2.48 (m, 4 H)	2.53 (m, 4 H)	3.09 (m, 4 H)
8-H_B	2.48 (m, 4 H)	2.53 (m, 4 H)	2.71 (m, 4 H)
9-H_A	1.49 (m, 4 H)	1.49 (m, 4 H)	1.93 (m, 4 H)
9-H_B	1.49 (m, 4 H)	1.49 (m, 4 H)	1.69 (m, 4 H)
10-H	2.48 (m, 8 H)	2.47 (m, 8 H)	2.96 (m, 8 H)
7-H	−	−	4.77 [m (t), 4H]
11-H	−	−	5.03 [m (t), 2H]

[a] ^1J = 16 Hz; ^2J = 7 Hz. [b] ^1J = 16 Hz; ^2J = 3 Hz.

Table 7. Comparison of the ^{13}C NMR spectra (δ [ppm], [D_6]DMSO) of the free ligand **4**, its sodium dipyrazolate salt **4′** and the Zn^{II} dipyrazolate complex [**12**]$(ClO_4)_2$

	4 (1)	**4′** (2)	Δδ (2−1)	{[**12**]$(ClO_4)_2$} (3)	Δδ (3−2)
C-3,5	146.97[a]	147.31[b]	0.34	151.12[b]	3.81
C-4	101.71	100.58	−1.13	96.88	−3.70
C-6	45.27	46.26	0.99	45.90	−0.36
C-8	47.02	47.14	0.12	50.67	3.56
C-9	29.22	29.26	0.04	23.72	−5.94
C-10	47.67	47.78	0.11	49.96	2.18

[a] Broad signal. [b] Sharp singlet.

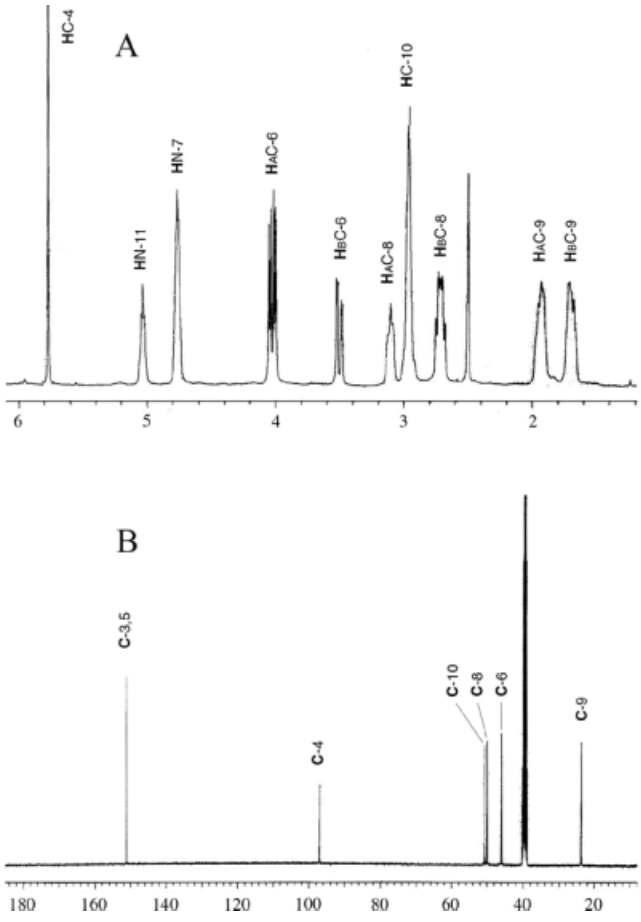

Figure 3. ^1H (A) and ^{13}C (B) NMR spectra of the Zn^{II} complex {[**12**]$(ClO_4)_2$} in [D_6]DMSO solution

moieties, appear in the spectrum as an AB spin system (Figure 3) suggesting that Zn^{II} coordination confers a rigid structure on the complex. Except for the 4-H pyrazole proton, all the other protons belonging to the macrocyclic cavity of **12** exhibit a generalised downfield chemical shift of their signals. It is interesting to note that in the ^1H NMR spectrum appear two signals at $\delta = 4.77$ and $\delta = 5.03$ ppm, which are attributable to the protons of the amino groups 7-H and 11-H, respectively. The triplet-like shape of these signals can be ascribed to their coupling with the neighbour methylene groups.

Table 7 shows the ^{13}C NMR signals of **4**, **4′** and [**12**]$(ClO_4)_2$ as well as the variations in the chemical shifts due to deprotonation of the pyrazole moieties which leads to **4′** [$\Delta\delta$ (2−1)] and the formation of the dinuclear Zn^{II} complex **12** [$\Delta\delta$ (3−2)].

In [D_6]DMSO, the C-3,5 quaternary carbon atoms of the free ligand **4** appear in the spectrum as a broad signal, while in the spectrum of **4′** this signal changes to a sharp singlet indicating that the slow prototropic equilibrium of the pyrazole rings has disappeared. Furthermore, as can be expected, upfield (δ =1.13 ppm for C-4) and downfield (δ = 0.34 ppm for C-3,5) variations of the pyrazole carbon signals confirm the formation of pyrazolate anions (Table 7).

Taking the ^{13}C NMR signals of **4′** as a reference, it can be observed that formation of the Zn^{II} dipyrazolate complex **12** induces strong downfield shifts in the signals of all the carbon atoms located in the α- positions to the nitrogen atoms involved in the complexation of the Zn^{II} ions. It also exerts strong upfield shifts on the signals of those located in the β- positions (Table 7).

*Crystal Structure of [$Cu_2(H_{-2}L^4)$]$(ClO_4)_2$ {[**11**]$(ClO_4)_2$}*

The crystallographic data were recorded at 150 K because some disorder found within the propylenic chains of the bridges and in the perchlorate counter anions prevented a satisfactory solution of the crystal structure from data collected at room temperature. Although even at low temperature some disorder persists, the solution is good enough for unequivocally identifying the structural characteristics of the coordination sites.

Crystals of [**11**]$(ClO_4)_2$ consist of $[Cu_2(H_{-2}\mathbf{L^4})]^{2+}$ cations and perchlorate anions. The coordination geometry around each copper atom is an irregular, axially elongated square pyramid. The base of the pyramid is formed by the two secondary nitrogen atoms of the polyamine bridge closer to the heterocycle and by two nitrogen atoms of two different pyrazolate units which act as $\eta^1{:}\eta^1$ bis(monodentate) anionic bridging ligands (Figure 4). The displacements of the metal ions from the plane of the nitrogen donors are 0.322(2) Å for Cu1 and 0.303(2) Å for Cu2. The central nitrogen atoms of the bridges occupy the axial positions. In both coordination sites, the Cu−N distances involving the sp^2 pyrazolate nitrogen atoms [Cu(1)−N(3) = 1.963(9) Å, Cu(2)−N(4) = 1.94(1) Å; Table 8] are much shorter than those of the secondary nitrogen atoms [Cu(1)−N(2) = 2.10(1) Å, Cu(2)−N(5) = 2.11(1) Å]. The Cu(1)−Cu(2) distance is 3.96 Å which is almost identical to those found in the crystal structures of $[Cu_2(H_{-2}\mathbf{L^1})](ClO_4)_2$ {[**5**]$(ClO_4)_2$}[17,11] and $[Cu_2(H_{-1}\mathbf{L^2})](ClO_4)_3{\cdot}2H_2O$ {[**6**]$(ClO_4)_2(HClO_4){\cdot}2H_2O$}[11] as well as in several crystal structures of other pyrazole-containing complexes in which the pyrazolate anions exhibit the same coordination mode.[8,15,16] However, such a distance is not so fixed in some complexes of podand ligands containing pyrazole bridges.[22] It is also interesting to point out that the axial

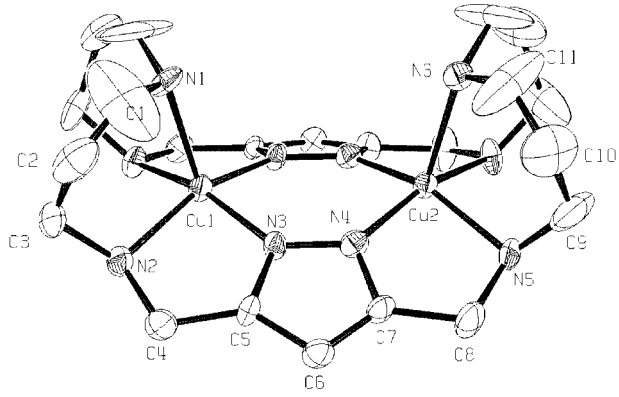

Figure 4. ORTEP drawing for the cation $[Cu_2(H_{-2}\mathbf{L^4})]^{2+}$ (**11**); thermal ellipsoids are drawn at the 30% probability level

Table 8. Selected bonds lengths [Å] and angles [°] of [**11**]$(ClO_4)_2$

Parameter	Length/angle
Cu1−N1	2.20(2)
Cu1−N2	2.1(1)
Cu1−N3	1.963(9)
Cu2−N4	1.94(1)
Cu2−N5	2.11(1)
Cu2−N6	2.24(2)
N1−Cu1−N2	92.6(5)
N1−Cu1−N3	106.8(5)
N2−Cu1−N3	80.5(4)
N4−Cu2−N5	81.1(4)
N4−Cu2−N6	106.4(4)
N5−Cu2−N6	91.7(5)

elongation observed in this complex is much smaller than those previously reported for $[Cu_2(H_{-2}\mathbf{L^1})](ClO_4)_2$ and $[Cu_2(H_{-1}\mathbf{L^2})](ClO_4)_3{\cdot}2H_2O$.[11] The complex again adopts a boat-shaped conformation with the side-chains folded towards the same side of the macrocyclic cavity.

Crystal Structure of [$Zn_2(H_{-2}L^4)$]$(ClO_4)_2$ {[12]$(ClO_4)_2$}

The crystallographic data were also recorded at 150 K because similar disorder to that found in the previous case was observed and this prevented a satisfactory solution from data recorded at room temperature. Crystals of [**12**]$(ClO_4)_2$ consist of $[Zn_2(H_{-2}\mathbf{L^4})]^{2+}$ cations and perchlorate anions. The coordination geometry around each Zn^{II} atom is very irregular and can be defined as a distorted square pyramid. Analogous to the previous structure, the base of the pyramid is formed by the two secondary nitrogen atoms of the polyamine bridge closer to the heterocycle and by two nitrogen atoms of two different pyrazolate units which act as $\eta^1{:}\eta^1$ bis(monodentate) anionic bridging ligands (Figure 5). The displacements of the metal atoms above the plane defined by the nitrogen donors are 0.595(2) Å for Zn1 and 0.554(2) Å for Zn2. The central nitrogen atoms of the polyamine bridges occupy the axial positions which in this case do not show any distortion. In contrast to the analogous Cu^{II} complex, the Zn−N distances of the sp^2 pyrazole nitrogen atoms in this case [Zn(1)−N(3) = 2.037(9) Å, Zn(2)−N(4) = 2.040(8) Å; Table 9] are close to those of their secondary nitrogen atoms in the centre of the bridge [Zn(1)−N(1) = 2.08(1) Å, Zn(1)−N(2) = 2.09(1) Å]. The largest M−N distances are found for the secondary nitrogen atom adjacent to the heterocycle. The Zn(1)−Zn(2) distance is again 3.96 Å confirming that it is fixed by the pyrazolate bridge. The conformation of the whole molecule is again boat-shaped with the central part of both chains folded towards the same side of the macrocyclic plane (Figure 5).

Table 9. Selected bonds lengths [Å] and angles [°] of [**12**]$(ClO_4)_2$

Parameter	Length/angle
Zn1−N1	2.08(1)
Zn1−N2	2.206(8)
Zn1−N3	2.037(9)
Zn2−N4	2.040(8)
Zn2−N5	2.196(8)
Zn2−N6	2.09(1)
N1−Zn1−N2	99.5(4)
N1−Zn1−N3	114.3(4)
N2−Zn1−N3	77.4(3)
N4−Zn2−N5	77.38(3)
N4−Zn2−N6	112.7(3)
N5−Zn2−N6	98.1(3)

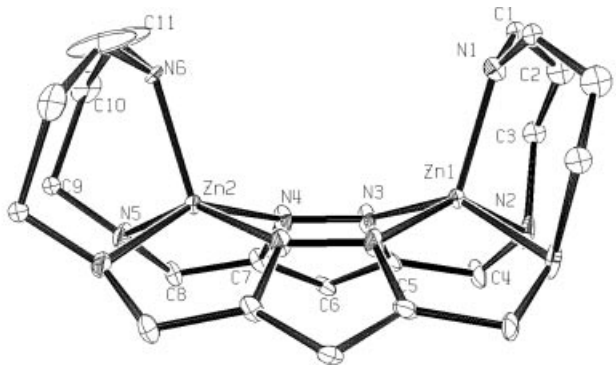

Figure 5. ORTEP drawing for the cation $[Zn_2(H_{-2}\mathbf{L^4})]^{2+}$ (**12**); thermal ellipsoids are drawn at the 30% probability level

Synthesis of Cu^{II} Dipyrazolate Complexes[$Cu_2(L^4)$]$(ClO_4)_4{\cdot}2H_2O$ {[13]$(ClO_4)_4{\cdot}2H_2O$} and [$Cu_3(H_{-2}L^4)$]$(ClO_4)_4{\cdot}2MeOH$ {[14]$(ClO_4)_4{\cdot}2MeOH$} from L^4

Synthesis and Spectroscopic Characterisation

It is interesting to point out that when we tried to obtain the dipyrazolate complexes $[Cu_2(H_{-2}\mathbf{L^4})](ClO_4)_2$ {[**11**]$(ClO_4)_2$} by direct treatment of the neutral ligand **4** with $Cu(ClO_4)_2{\cdot}6H_2O$ in methanol, we observed very different behaviour to that previously described using the disodium dipyrazolate salt **4′** as a starting material. Thus, treatment of a methanolic solution of **4** (2.5×10^{-2} M) with $Cu(ClO_4)_2{\cdot}6H_2O$ (2 equiv.) at room temperature gave a blue precipitate which, after being vacuum-dried at 100 °C, afforded a blue solid of formula $[Cu_2\mathbf{L^4}](ClO_4)_4{\cdot}2H_2O$ in 71% yield. After redissolving this blue solid in boiling water for 5 min, a red solid slowly and unexpectedly crystallised. After being vacuum-dried at 100 °C, this resulted in a reddish-brown complex of formula $[Cu_2\mathbf{L^4}](ClO_4)_4{\cdot}2H_2O$ {[**13**]$(ClO_4)_4{\cdot}2H_2O$} (Scheme 3) in 61% yield. Surprisingly, this red complex had identical analytical data to the blue precursor mentioned above. Microanalysis performed by X-ray energy dispersive spectrometry confirmed the proposed Cu/Cl ratio. This can be explained if both the blue and the red forms of this complex correspond to dinuclear Cu^{II} dipyrazolate species which share the characteristic feature of having the two sp^3 nitrogen atoms located at the centre of the side chains protonated and, in contrast to $[Cu_2(H_{-2}\mathbf{L^4})](ClO_4)_2$ {[**11**]$(ClO_4)_2$}, thereby not directly coordinated to the metal atoms (Scheme 3). The coordination

of the metal ion causes the release of the protons from the pyrazole fragments which are captured by the basic central nitrogen atoms of the bridges.

Furthermore, the ESI-MS data of either the precursor blue form or the red final form show identical peaks which appear with different relative abundances as shown in Table 10. In the negative mode, the molecular ion $[M - H]^-$, corresponding to $[Cu_2(H_{-1}\mathbf{L^4})(ClO_4)_4]^-$ appears at m/z = 969.4 with low relative abundance (see Table 10), together with a more intense peak at m/z = 1071.4 and the base peak at m/z = 869.4 assignable to the species $[M + ClO_4]^-$ and $[(M - ClO_4 - 2\ H]^-$, respectively, which agree with the proposed structure. Moreover, in the positive mode, two characteristic peaks appear at m/z = 871 and 771, assignable to the $[Cu_2(\mathbf{L^4})(ClO_4)_3]^+$ and $[Cu_2(H_{-1}\mathbf{L^4})(ClO_4)_2]^+$ species which correspond to dinuclear Cu^{II} dipyrazolate fragments containing partly protonated polyamine chains. On the other hand, in addition to the expected peak at m/z = 671 assignable to the most abundant fragment $[(H_{-2}\mathbf{L^4})Cu_2(ClO_4)]^+$, both the precursor blue and the final red forms of $[\mathbf{13}](ClO_4)_2(H_2O)_2$ show a characteristic peak at m/z = 547 attributable to $[(H_2\mathbf{L^4})(ClO_4)]^+$ which demonstrates the presence of protonated nitrogen atoms in the ligand structure.

Table 10. Comparison of the most significant peaks recorded in the ESI-MS data of the dinuclear Cu^{II} complex $\{[\mathbf{13}](ClO_4)_4{\cdot}2(H_2O)\}$ (1007.6) in both its blue and red forms

m/z	Composition	% blue	% red
Negative mode			
1071	$\{[Cu_2\mathbf{L^4}](ClO_4)_5\}^-$	35	14
969	$\{[Cu_2(H_{-1}\mathbf{L^4})](ClO_4)_4\}^-$	6	8
869	$\{[Cu_2(H_{-2}\mathbf{L^4})](ClO_4)_3\}^-$	100	100
Positive mode			
871	$\{[Cu_2\mathbf{L^4}](ClO_4)_3\}^+$	10	3
771	$\{[Cu_2(H_{-1}\mathbf{L^4})](ClO_4)_2\}^+$	10	4
671	$\{[Cu_2(H_{-2}\mathbf{L^4})](ClO_4)\}^+$	100	59
569	$[Cu_2(H_{-3}\mathbf{L^4})]^+$	3	4
547	$\{[H_2\mathbf{L^4}](ClO_4)\}^+$	51	33
447	$[H\mathbf{L^4}]^+$	–	41
224	$[(\mathbf{L^4}/2)+H]^+$	–	100

Unfortunately, up to now, it has not been possible to obtain adequate crystals of either the precursor blue form or the red form suitable for X-ray analysis.

However, on the basis of the above observations, the colour changes observed can be tentatively attributed to the presence of the two water molecules which are bound in a different manner in both complexes. In the blue form they would be coordinated to the metal ion occupying the axial positions of the pentacoordinate environment (see Scheme 4, blue-[**13**]). In the red form the coordination environment around each Cu^{II} will be square-planar and the water molecules would not occupy the first coordination sphere of the metal ion (Scheme 4, red-[**13**]). In both cases the water molecules might be stabilised through $^+NH\cdots OH_2$ hydrogen bonds with the two protonated sp^3 nitrogen atoms located in the centre of the side chains. We previously reported these types of monohydrated ammonium groups in the crystalline structure of the dinuclear Cu^{II} complex $[\mathbf{6}](HClO_4)(ClO_4)_2{\cdot}2H_2O$[11] where one of the aliphatic nitrogen atoms of the noncoordinated bridge is protonated and hydrogen-bonded to a water molecule.

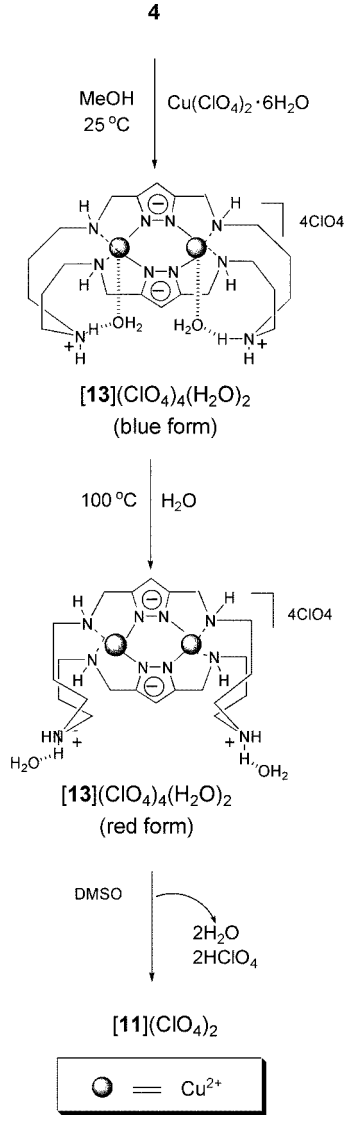

Scheme 4

In the complex $\{\text{red-}[\mathbf{13}](ClO_4)_2{\cdot}2H_2O\}$, the conformational change produced would be induced by the treatment of the starting precursor blue form with boiling water.

Finally, when we tried to obtain similar dinuclear complexes starting from a more concentrated solution of ligand $\mathbf{L^4}$ (**4**) (6.0×10^{-2} M) under similar reaction conditions [2 equiv. of $Cu(ClO_4)_2{\cdot}6H_2O$ at room temp.], we obtained another unexpected result. A bright green solid precipitated from the methanol solution which, after being vacuum-dried at 100 °C, gave a new trinuclear copper complex in low yield (28%). The analytical and MS data of this new complex are consistent with the formula $[Cu_3(H_{-2}\mathbf{L^4})](ClO_4)_4{\cdot}2MeOH$ $\{[\mathbf{14}](ClO_4)_4{\cdot}2MeOH\}$

(Scheme 3). The Cu/Cl (3:4) molar ratio was confirmed by X-ray energy dispersive spectrometry.

Since matrix-assisted laser desorption/ionisation (MALDI-TOF) mass spectrometry is actually among the most important ionisation methods for strong metal-ion complexes,[23] we used this technique in order to confirm the structure of the trinuclear complex. Table 11 shows the most significant trinuclear copper ions detected in the MALDI-TOF mass spectrum of {[**14**]$(ClO_4)_4$·2MeOH} using 2,5-dihydroxybenzoic acid (DHB) as a matrix. In a similar way as has already been observed in other MALDI-TOF mass spectra of copper complexes in which Cu^{II} ions are apparently simply reduced,[24,25] the composition of most of the ionic fragments gathered in Table 11 agree with different copper oxidation states due to partial or total copper reduction processes for which the source of the electrons may be the photoionised DHB matrix. Thus, at *m*/*z* = 635 appears the base peak corresponding to the skeletal trinuclear copper fragment $[Cu_3(H_{-2}\mathbf{L^4})]^+$ in which the three Cu^{II} atoms are reduced to Cu^{I}. Other characteristic ions which correspond to the proposed structure appear at *m*/*z* (%) = 734.3 (78) and 797.2 (27). Both peaks are attributable to the ionic species $[Cu_3(H_{-2}\mathbf{L^4})(ClO_4)]^+$ and $[Cu_3(H_{-2}\mathbf{L^4})(MeO)(MeOH)]^+$, respectively, in which two of the three Cu^{II} atoms have been reduced to Cu^{I}. The last mentioned species (*m*/*z* = 797.2) confirms the presence of two MeOH molecules in the complex and simultaneously suggests that one of these molecules may be acting as a bridge between two copper ions.

Table 11. Most significant peaks recorded in the MALDI-TOF-MS of [**14**]$(ClO_4)_4$·2MeOH corresponding to trinuclear copper fragments

m/*z* (%)	Composition[a]	Oxidation state
797.2 (27)	$\{[Cu_3(H_{-2}\mathbf{L})](MeO)(MeOH)\}^+$	2 Cu^+ + Cu^{2+}
750.3 (7)	$\{[Cu_3(H_{-2}\mathbf{L})](ClO_4)+(O)\}^+$	3 Cu^{2+}
734.3 (78)	$\{[Cu_3(H_{-2}\mathbf{L})](ClO_4)\}^+$	2 Cu^+ + Cu^{2+}
649.4 (26)	$\{[Cu_3(H_{-4}\mathbf{L}) +(O)]\}^{\cdot+}$	3 Cu^{2+}
635.4 (100)	$[Cu_3(H_{-2}\mathbf{L})]^+$	3 Cu^+

[a] [$(H_{-2}\mathbf{L})$ = ($C_{22}H_{40}N_{10}$) and $(H_{-4}\mathbf{L})$=($C_{22}H_{38}N_{10}$)].

Finally, at *m*/*z* = 750.3 and 649.4 are two peaks assignable to ionic fragments containing oxygen in which the Cu^{II} initial oxidation state has not changed. However, it is difficult to be certain if these ions are truly formed or are the result of secondary oxidation reactions in the matrix as was previously observed in other MALDI-TOF mass spectra of metallic complexes.[25]

Molecular Modelling Studies

In order to gain further insight into the molecular structures of both the dinuclear Cu^{II} [**13**]$(ClO_4)_4$·$2H_2O$ and the trinuclear Cu^{II} complex {[**14**]$(ClO_4)_4$·2MeOH}, we performed some modelling studies. Molecular mechanics models of complexes of a variety of metal ions have been recently developed[26] and have proved useful for ligand design. Use of a well-established biochemically oriented force field with specific metal parameters would allow the interactions of metal complexes and biological molecules to be studied and modelled. Among the well-established force-fields, AMBER[27] has found widespread use in the modelling of biological molecules and the development of suitable parameter sets which allows the modelling of metal complexes. This has produced results in good agreement with experimental observations without requiring additional changes.[28] For those reasons, in this work, molecular modelling studies were carried out using the AMBER method modified by the inclusion of appropriate parameters.

To check the consistency of the calculations we modelled the complex [**11**]$(ClO_4)_2$ (which has a known X-ray structure) according to the same procedure detailed in the Exp. Sect. with no restraints. Data obtained in this modelling study agree quite well with the crystallographic results, although the calculated Cu−Cu distances are shorter than the experimentally measured ones (0.12 Å, similar to maximum deviation obtained by Comba et al.).[29]

To study the copper complexes [**13**]$(ClO_4)_4$·$2H_2O$ and [**14**]$(ClO_4)_4$·MeOH, coordination numbers and geometries were selected according to the preferences of copper(II) and, taking into account all the experimental data for the synthesised complexes, red-[**13**] was assumed to be square-planar while blue-[**13**] and green [**14**] were assumed to be pyramidal. Thus, we modelled the blue and red forms of the dihydrated complex [**13**]$(ClO_4)_4$·$2H_2O$ with the results given in Figure 6 (A).

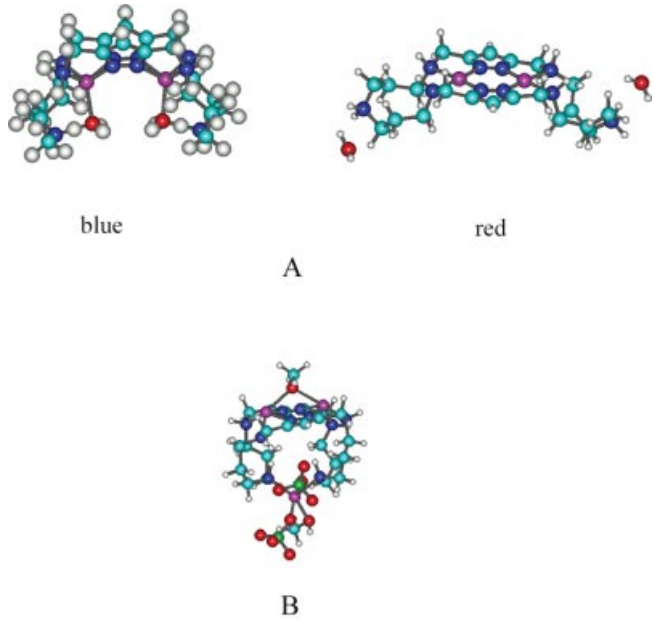

Figure 6. A) Molecular models of the blue and red forms of the complex [**13**]$(ClO_4)_4(H_2O)_2$; B) molecular model for the trinuclear complex [**14**]$(ClO_4)_4(MeOH)_2$

In the above complexes, the calculated Cu−Cu distance between the two metal ions coordinated with pyrazole ni-

trogen atoms is 3.52 Å for the red form of [**13**], denoting the rigidity of the bridge, and 4.03Å for its blue form which is more similar to the values found for [**11**] (calculated 3.84 Å, X-ray data 3.96 Å).

Since they have different connectivities, no attempt was made to compare the calculated molecular mechanics strain energies of the different coordination complexes since each one needs a different parameter set. PM3 calculations of the corresponding heats of formation, however, suggests that the red form of {[**13**]$(ClO_4)_4$·$2H_2O$} is more stable than the blue one.

Finally, a model for the green trinuclear Cu^{II} complex [**14**]$(ClO_4)_4$·2MeOH is given in Figure 6 (B). Coordination of the metal centres to the pyrazole sp^2 nitrogen atoms and the adjacent nitrogen atoms forces the central parts of both bridges to move upwards in the same direction thereby enabling the central nitrogen atoms to coordinate to a further metal ion provided there are other ancillary ligands that can assist the processes. In this case the methanol molecules could complete the coordination spheres. In [**14**], the calculated Cu−Cu distances between the third metal ion and the pyrazole-coordinated metal ion are 5.89 Å and 6.41 Å, respectively, while the distance between these two remains quite similar to that of 3.83 Å in the blue form of [**13**].

^{1}H NMR Spectra of {red-[13]$(ClO_4)_4$·$2H_2O$}

In order to obtain further information about the nature of the red complex $[Cu_2\mathbf{L^4}](ClO_4)_4$·$2H_2O$ {red-[**13**]$(ClO_4)_4$·$2H_2O$} (Scheme 3), we performed paramagnetic ^{1}H NMR spectroscopy. This technique is very useful for the study of magnetically coupled systems such as dinuclear Cu^{II}−Cu^{II} complexes.[30,31] However, in the case of mononuclear Cu^{II} complexes its usefulness is rather limited due to the large electronic relaxation time of Cu^{II} which consequently produces a large broadening of the signals. The information that this technique provides refers to the electronic properties, coordination geometry and conformational changes in solution.

The ^{1}H NMR spectrum of the red $[Cu_2\mathbf{L^4}](ClO_4)_4$·$2H_2O$ complex in $(CD_3)_2SO$ is shown in Figure 7 (A). It displays, in the downfield region, nine hyperfine-shifted signals (a−i) and four other signals (j−m) which are shifted upfield. When the temperature is raised up to 45 °C, the broad signals a−c and e move upfield, Figure 7 (B, C). This change is irreversible and at the same time the colour of solution changes from red-violet to blue, indicating a conformational change. The isotropically shifted resonances, longitudinal relaxation times (T_1) and line widths at half-height are reported in Table 12 for the red complex $[Cu_2\mathbf{L^4}](ClO_4)_4$·$2H_2O$ {red-[**13**]$(ClO_4)_4$·$2H_2O$}. The above-mentioned signals (a−c) display short T_1 values (< 1 ms) and broad line widths at half-height of around 2000 Hz. This, together with the proton integrations, permits the assignment of these signals to the protons of the CH_2 groups located α to the coordinated nitrogen atoms nearest to the Cu^{II} ion (see Scheme 5). When the temperature is raised up to 45 °C (see Figure 7, C), the broad signals which move upfield integrate for eight more protons, indicating an increase in the coordination number of the copper ion. In this sense, signal (e) which integrates for eight protons and can

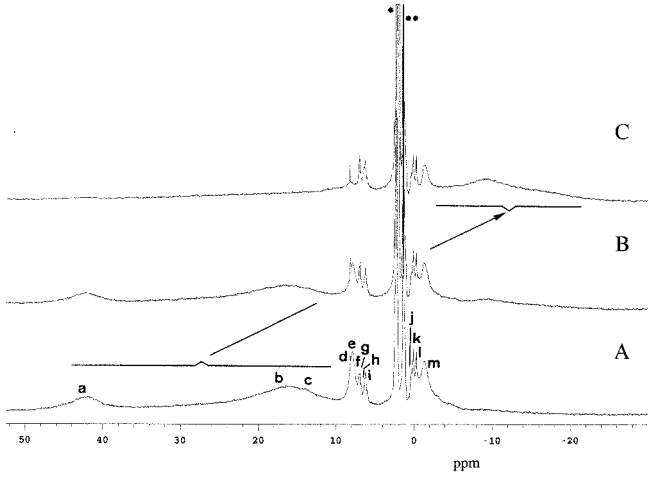

Figure 7. 400 MHz ^{1}H NMR spectra of $[Cu_2\mathbf{L^4}](ClO_4)_4(H_2O)_2$ in $(CD_3)_2SO$ at different temperatures: 298 K (A); 313 K (B); 323 K (C); the asterisks mark the residual solvent and impurity signals [* $(CH_3)_2SO$; ** HOD]

Table 12. ^{1}H NMR hyperfine-shifted resonances of red-[**13**]$(ClO_4)_4$·$2H_2O$ in $(CD_3)_2SO$ at 298 K

Signal	δ [ppm]	Assignments	Number of protons	T_1 [ms]	$\Delta\nu_{1/2}$ [Hz]	T_2 [ms][a]
a	42.3	α-CH_2		< 1	1740	0.18
b	15.8	α-CH_2	16	< 1	2128	0.15
c	14.2	α-CH_2		< 1	[b]	[b]
d	8.2	$H_{pyrazole}$[c]	1	138	52[d]	6.1[d]
e	7.8	γ-CH_2	8	108	[b]	[b]
f	7.1	$H_{pyrazole}$[c]	1	146	[b]	[b]
g	6.9	β-CH_2		146	[b]	[b]
h	6.4	β-CH_2		150	[b]	[b]
i	6.2	β-CH_2		152	[b]	[b]
j	0.27	β-CH_2	8	130	[b]	[b]
k	0.05	β-CH_2		158	[b]	[b]
l	−0.32	β-CH_2		158	65[d]	4.9[d]
m	−1.4	β-CH_2		114	322[d]	1.0[d]

[a] Measured from the line width at half-height. [b] Overlap prevents measurement of this value. [c] Tentative assignments. [d] Measured at 323 K (blue complex).

be assigned to CH_2 groups located γ to the coordinated nitrogen atoms in the red-violet $[Cu_2\mathbf{L^4}](ClO_4)_4{\cdot}2H_2O$ {red-[**13**]$(ClO_4)_4{\cdot}2H_2O$} complex, disappears completely in the ^{1}H NMR spectrum of the blue complex **13**. These results clearly illustrate a change in the coordination geometry from square-planar in the red form to pyramidal or five-coordinate in the blue form. The data also suggest that in the blue form, the nitrogen atoms in the centre of the bridges are coordinated to the metal ion. Therefore, in the weakly acidic solvent $(CD_3)_2SO$, the centre nitrogen atoms are deprotonated and the red complex gradually transforms to $[Cu_2(H_{-2}\mathbf{L^4})]^{2+}$ (**11**) (see Scheme 5). Indeed, this spectrum is identical to that obtained of a solution formed by directly dissolving $[Cu_2(H_{-2}\mathbf{L^4})](ClO_4)_2$ ([**11**]$(ClO_4)_2$] in the same solvent. The other signals (d and f−m), which correspond to the CH_2 groups β to the coordinated nitrogen atoms and to the pyrazole protons, display large T_1 values (100−150 ms). As described previously,[31] dinuclear Cu^{II} complexes have similar T_1 values and broad line widths.

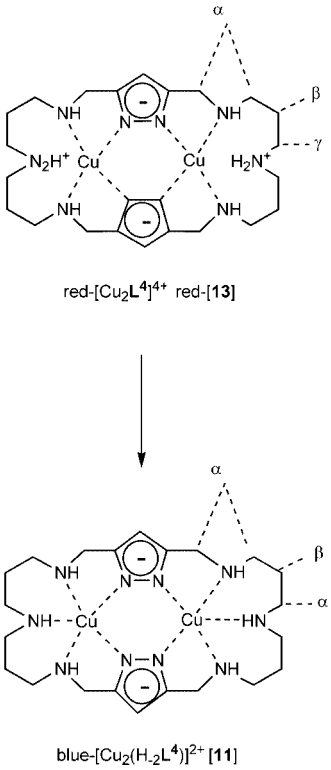

Scheme 5

In addition, variable-temperature ^{1}H NMR spectra of red-$[Cu_2\mathbf{L^4}](ClO_4)_4{\cdot}2H_2O$ were recorded from 293 to 323 K. The representation of the temperature dependence of the paramagnetic hyperfine-shifted resonances for some protons is shown in Figure 8. All signals are temperature-independent except for signals (a) and (b). Only signal (a) exhibits anti-Curie behaviour and furthermore signal (b) shows Curie behaviour. Extrapolated values at infinite temperatures for signal (a) indicate the existence of magnetic coupling.[31]

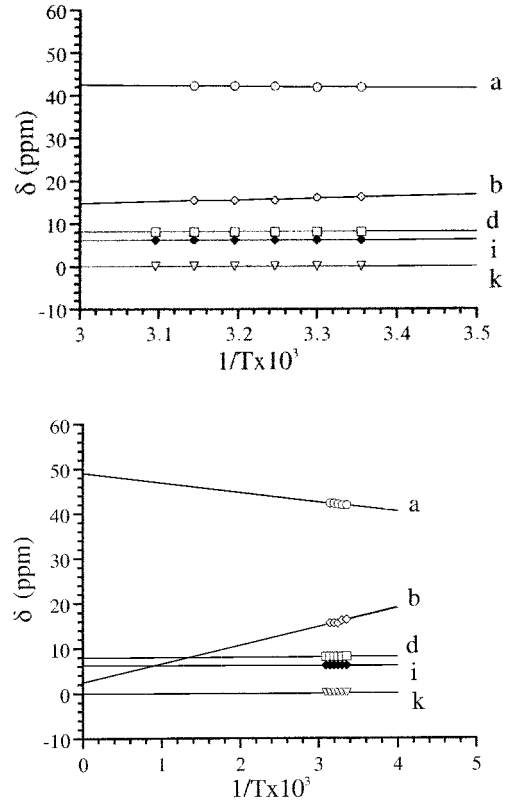

Figure 8. Temperature dependence of the isotropically shifted resonances of red-[**13**]$(ClO_4)_4{\cdot}2H_2O$; the insert shows the plot with the $1/T$ coordinate expanded

Magnetic Measurements of {red-[13] $(ClO_4)_4{\cdot}2H_2O$} and {[11] $(ClO_4)_2$}

The magnetic properties of $[Cu_2(H_{-2}\mathbf{L^4})](ClO_4)_2$ {[**11**]$(ClO_4)_2$} and $[Cu_2(\mathbf{L^4})](ClO_4)_4{\cdot}2H_2O$ {red-[**13**]$(ClO_4)_4{\cdot}2H_2O$} are shown in Figure 9 in the form of $\chi_M T$ versus T, χ_M being the magnetic susceptibility per two copper(II) ions. The value of $\chi_M T$ at room temperature is 0.46 $cm^3{\cdot}mol^{-1}$ K for $[Cu_2\mathbf{L^4}](ClO_4)_4{\cdot}2H_2O$ and $[Cu_2(H_{-2}\mathbf{L^4})](ClO_4)_2$, a value which is significantly lower than that expected for two uncoupled Cu^{II} ions. Upon cool-

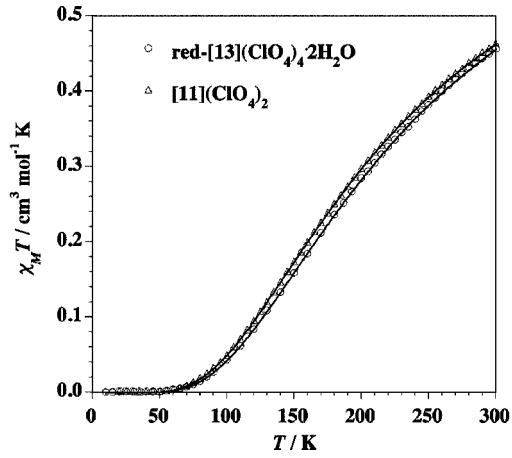

Figure 9. Plot of $\chi_M T$ vs. T for the complexes red-[**13**]$(ClO_4)_4{\cdot}2H_2O$ and [**11**]$(ClO_4)_2$

ing $\chi_M T$ continuously decreases, vanishing at around 70 K. Moreover, the corresponding χ_M curves show maxima at 270 K (for $[Cu_2\mathbf{L^4}](ClO_4)_4{\cdot}2H_2O$) and 255 K (for $[Cu_2(H_{-2}\mathbf{L^4})](ClO_4)_2$] (see Supporting Information, Figure S2). This magnetic behaviour is characteristic of an important antiferromagnetic interaction between the Cu^{II} ions with singlet spin ground states.

We have interpreted the magnetic data according to the actual dinuclear nature of the complexes with the spin Hamiltonian $\mathbf{H} = -J\mathbf{S_1S_2}$. The fit of the magnetic data to the appropriate susceptibility expression derived from the van Vleck formula and assuming that the *g* factors for both Cu^{II} ions are identical, leads to $J = -299(7)$ cm^{-1} and $g = 2.09(1)$ for red-$[Cu_2\mathbf{L^4}](ClO_4)_4{\cdot}2H_2O$ {red-**[13]**$(ClO_4)_2{\cdot}2H_2O$}, and $J = -286(6)$ cm^{-1} and $g = 2.07(1)$ for $[Cu_2(H_{-2}\mathbf{L^4})](ClO_4)_2$ {**[11]**$(ClO_4)_2$}.

The observed *J* values lie in the upper range of the magnetic interactions found for related bis(μ-pyrazolato)-bridged dinuclear complexes. In fact, to the best of our knowledge, the highest *J* value observed for this family is $J = -412$ cm^{-1} for the compound $[Cu_2\mathbf{L^2}](BF_4)_2$ where L = 3,5-bis(*i*PrSCH$_2$)pyz.[32] The existence of σ-donor atoms as peripheral ligands may be responsible for these strong interactions.[33] However, the number of structurally characterised examples reported in the literature is still limited.[34]

The pathway for magnetic exchange is propagated through the bridging pyrazolate ligands. From the molecular structure of $[Cu_2(H_{-2}\mathbf{L^4})](ClO_4)_2$ {**[11]**$(ClO_4)_2$} one can conclude that the unpaired electron in each metal centre is clearly described by a $d_{x^2-y^2}$ magnetic orbital which is coplanar with the pyrazolate skeleton. The significant overlap between these magnetic orbitals accounts for the strong antiferromagnetic coupling observed. Although the crystal structure of $[Cu_2\mathbf{L^4}](ClO_4)_4{\cdot}2H_2O$ is not available, the very close magnetic behaviour of the complexes $[Cu_2\mathbf{L^4}](ClO_4)_4{\cdot}2H_2O$ {red-**[13]**$(ClO_4)_4{\cdot}2H_2O$} and $[Cu_2(H_{-2}\mathbf{L^4})](ClO_4)_2$ allows us to predict a similar exchange pathway. This again supports the suggestion that deprotonation of the pyrazole rings has occurred in both structures.

Conclusions

The synthesis of a 2+2 polyamine macrocycle containing pyrazole spacers connected through methylene groups to dipropylenetriamine bridges (**L^4**) has been described here for the first time. The acid-base behaviour of **L^4** in water reveals that, like the analogous macrocycle containing diethylenetriamine bridges (**L^1**), the pyrazole spacers do not participate in any net protonation step in the pH range of 2−11. The number of protonation steps observed is equal to the number of amino groups in the bridges. ^{1}H and ^{13}C NMR spectroscopy support this conclusion. The overall basicity of **L^4** is, on the other hand, five orders of magnitude greater than that of **L^1**. The deprotonation of the pyrazole moieties can, however, be readily achieved in the presence of coordinated metal ions. Cu^{II} induces the deprotonation of the pyrazole rings at lower pH values than Zn^{II} due to its much stronger interaction with the ligand. On the other hand, pyrazole deprotonation is more readily achieved (at more acidic pH values) with the ligand **L^1** bearing ethylenic chains in the bridges with five-membered chelates than in **L^4** containing six-membered chelates and a higher overall basicity.

The higher basicity of **L^4** is also reflected in the different syntheses of the dinuclear solid complexes which we have carried out. In the case of **L^1**, treatment of $Cu(ClO_4)_2{\cdot}6H_2O$ with either neutral **L^1** or with its disodium salt $Na_2[H_{-2}\mathbf{L^1}]$ in ethanol followed by crystallisation from water leads to the formation of the same dinuclear complex $[Cu_2(H_{-2}\mathbf{L^1})](ClO_4)_2$ in which the pyrazole groups are deprotonated thereby behaving as $\eta^1{:}\eta^1$ monodentate bridging ligands and the polyamine bridges are completely deprotonated. In the case of **L^4** the situation is different. Treatment of neutral **L^4** with $Cu(ClO_4)_2{\cdot}6H_2O$ in MeOH gives a blue solid complex which by heating in boiling water (for 5 min) followed by slow crystallisation leads to a red compound. The elemental analyses of both the blue and the red forms of this complex are consistent with the same empirical formula, i.e. $[Cu_2\mathbf{L^4}](ClO_4)_4{\cdot}2(H_2O)$. The ESI-MS and ^{1}H NMR paramagnetic data of the red complex clearly indicates that it is a dinuclear square-planar Cu^{II} complex in which the central nitrogen atoms of the bridging chains are not involved in the coordination to the metal ions and are therefore protonated. On the basis of both the elemental analysis of {red-**[13]**$(ClO_4)_4{\cdot}2H_2O$} and crystallographic data of polyamine receptors previously reported, it seems reasonable to suppose that the above-mentioned protonated nitrogen atoms may be hydrogen-bonded to water molecules [Scheme 4, **13** (red form)]. The blue form shows the same feature but in this case the coordination geometry should be pyramidal with the water molecules occupying the axial positions. The exchange between the two forms depends on both the temperature and the solvent. Therefore, the marked basicity of the propylamine chains facilitates the capture of the protons released from the pyrazole rings.

However, if $Cu(ClO_4)_2{\cdot}6H_2O$ is treated with the sodium salt $Na_2[H_{-2}\mathbf{L^4}]$ in methanol followed by crystallisation from water, the complex obtained is $[Cu_2(H_{-2}\mathbf{L^4})](ClO_4)_2$ {**[11]**$(ClO_4)_2$} which is analogous to that obtained with **L^1** (Scheme 3). The crystal structure of $[Cu_2(H_{-2}\mathbf{L^4})](ClO_4)_2$ shows a very irregular square-pyramidal coordination geometry in which the shorter distances are those involving the pyrazole nitrogen atoms and the axial ones are involved in both coordination sites by the central nitrogen atoms of the propylenic chains. Analogously, in the case of Zn^{II}, the crystal structures of $[Zn_2(H_{-2}\mathbf{L^1})](ClO_4)_2$ {**[8]**$(ClO_4)_2$} and $[Zn_2(H_{-2}\mathbf{L^4})](ClO_4)_2$ {**[12]**$(ClO_4)_2$} also reveal similar coordination arrangements. In the three structures, the overall shape of the complex cations is boat-like with the central parts of the polyamine bridges displaced towards the same side of the macrocyclic ring.

Finally, treatment of concentrated solutions of **L⁴** with $Cu(ClO_4)_2 \cdot 6H_2O$ gives a trinuclear complex of stoichiometry $[Cu_3(H_{-2}\mathbf{L^4})](ClO_4)_4 \cdot 2MeOH$ in low yield which has been characterised by MALDI-TOF mass spectrometry. The boat-like arrangement of the macrocycle in the dinuclear complex seems to facilitate the process.

Experimental Section

General: All starting materials were purchased from commercial sources (Aldrich) and used without further purification. Solvents were dried using standard techniques.[35] The organic reactions were monitored by thin layer chromatography (TLC) on precoated aluminium sheets of silica gel. Compounds were detected with iodine and/or with phosphomolybdic acid. Flash column chromatography was performed in the indicated solvent system on silica gel (particle size 0.040−0.063 mm). Melting points were determined with a Reichert-Jung hot-stage microscope. ^1H and ^{13}C NMR spectra were recorded with Varian Unity Inova-300, Varian Unity Inova-400 or Varian Unity 500 spectrometers at room temperature, employing D_2O or [D_6]DMSO as solvents. The pH was calculated from the measured pD values using the correlation pH = pD − 0.4.[36] Chemical shifts are reported in parts per million (ppm) from tetramethylsilane but were measured against the solvent signals. Dioxane (δ = 67.4 ppm) was used as reference for the ^{13}C NMR spectra in D_2O. All assignments were performed on the basis of ^1H-^{13}C heteronuclear multiple quantum coherence experiments (gHSQC and gHMBC). IR spectra were recorded with a Perkin−Elmer 681 spectrometer. EI mass spectra were recorded with a Hewlett Packard 5973 spectrometer with a direct insertion probe (70 eV). Electrospray mass spectra were obtained with a Hewlett Packard 1100 MSD and FAB mass spectra with a VG AutoSpec spectrometer using an *m*-nitrobenzyl alcohol (NBA) matrix. Elemental analyses were provided by the Departamento de Análisis, Centro de Química Orgánica "Manuel Lora Tamayo", CSIC, Madrid, Spain. Cu−Cl ratios were provided by the SCSIE (University of Valencia) using X-ray energy dispersive spectroscopy with an EDAX DX4 detector and a Philips XL30 ESEM electronic microscope.

Synthesis of Ligands: Ligands **L¹** (**1**), **L²** (**2**) and **L³** (**3**) were prepared by treatment of the corresponding 3,5-pyrazoledicarbaldehydes with diethylenetriamine [**L¹** (**1**) and **L³** (**3**)] or tris(2-aminoethyl)amine **L²** (**2**) as reported previously in refs.[10,11], respectively.

3,7,11,14,15,18,22,26,29,30-Decaazatricyclo[26.2.1.1^{13,16}]dotriaconta-1(31),13,16(32),28-tetraene [L⁴ (4)]: 3,5-Pyrazoledicarbaldehyde (496 mg, 4.0 mmol) was dissolved in hot dry methanol (200 mL). The solution was then cooled to room temperature and added dropwise under argon to a stirred solution of *N*-(3-aminopropyl)-1,3-propanediamine (525 mg, 4 mmol) in dry methanol (120 mL) over 2.5 h. The reaction was monitored by TLC ($CHCl_3$/MeOH, 10:1) and when it was complete (ca. 12 h), $NaBH_4$ (912 mg, 24.0 mmol) was added portionwise over 15 min. The mixture was stirred for 2 h and the solvent removed in vacuo. The residue was purified by flash column chromatography (MeOH/30% aqueous NH_4OH, 49:1 to 45:5 mixtures). The fractions containing the product of R_f = 0.65 (TLC, MeOH/30% aqueous NH_4OH, 1:1) were concentrated to dryness. The residue was then extracted with boiling toluene and on concentration and cooling gave **L⁴** (**4**) as an oil which was crystallised from toluene to give a white solid (443 mg, 49%) m.p. 154−156 °C. IR (KBr): $\tilde{\nu}$ = 3500−3300 cm^{-1} (NH). MS (FAB$^+$, 3-nitrobenzyl alcohol matrix): *m*/*z* (%) = 447 (100) [MH^+]. $C_{22}H_{42}N_{10}$ (446.6): calcd. C 59.16, H 9.48, N 31.36; found C 58.92, H 9.62, N 31.11.

Preparation of L⁴·6HCl (4·6HCl): A mixture of **L⁴** (**4**) (223 mg, 0.5 mmol) and 1 M aqueous hydrochloric acid (4 mL) was stirred for 12 h. After addition of EtOH (50 mL), a white precipitate formed which was filtered off and dried under reduced pressure for 48 h to give a white solid (319 mg, 91%); m.p. 265−268 °C. MS (ESI positive mode, H_2O): *m*/*z* (%) = 447 (100) [(M − 6 HCl)H$^+$]. $C_{22}H_{42}N_{10} \cdot 6HCl \cdot 2H_2O$ (701.4): calcd. C 37.67, H 7.47, N 19.97; found C 38.05, H 7.70, N 19.78.

Preparation of 4′ [Na₂(H₋₂L⁴)]: To a stirred solution of **4** (45 mg, 0.1 mmol) in dry MeOH (2 mL), was added NaOH (8 mg, 0.2 mmol), previously dissolved in MeOH (1 mL). The mixture was stirred at room temperature for 12 h. The solvent was then evaporated and the residue dried under reduced pressure for 48 h to give **4′** as a white solid (48 mg, 98%); m.p. 208−210 °C. MS (ESI positive mode, H_2O/MeOH): *m*/*z* (%) = 491.2 (10) [M + H]$^+$, 469.3 (76) [M + 2 H − Na]$^+$, 447.3 (100) [M + 3 H − 2 Na]$^+$. $C_{22}H_{40}N_{10}Na_2$ (490.6): calcd. C 53.86, H 8.21, N 28.54; found C 53.87, H 8.16, N 28.57.

Syntheses of $[Zn_2(H_{-2}L^1)](ClO_4)_2$ {[8](ClO₄)₂}, $[Zn_2(H_{-2}L^2)](ClO_4)_2 \cdot 4H_2O$ {[9](ClO₄)₂·4H₂O} and $[Zn_2(L^3)](ClO_4)_4 \cdot 6H_2O$ {[10](ClO₄)₄·6H₂O} from Ligands L¹−L³ (1−3). General Procedure: Working under argon, a solution of $Zn(ClO_4)_2 \cdot 6H_2O$ (74 mg, 0.2 mmol) in dry MeOH (1 mL) was added with stirring to a solution of the polyamine ligand L¹−L³ (0.1 mmol), dissolved in 2 mL of the same solvent. After 12 h, the precipitate was collected by filtration and vacuum-dried at 100 °C over phosphorus pentoxide for 24 h. In all cases, the white solid thus obtained was crystallised from water.

{[8](ClO₄)₂}: Yield 55 mg, 77%. M.p. > 350 °C. MS (ESI positive mode, H_2O): *m*/*z* (%) = 615.1 (10) [M − ClO_4]$^+$, 453.4 (100) [M + H − $Zn(ClO_4)_2$]$^+$, 391.4 (75) [M + 3 H − 2 $ZnClO_4$]$^+$. MS (FAB$^+$, 3-nitrobenzyl alcohol matrix): *m*/*z* (%) = 616.9 (20) [(M + 2 H)$^+$ − ClO_4], 615.4 (12) [M$^+$ − ClO_4], 553.2 (100) [(M + 2 H)$^+$ − $ZnClO_4$], 453.2 (47) [(M + H)$^+$ − $Zn(ClO_4)_2$]. $C_{18}H_{32}N_{10}Zn_2(ClO_4)_2$ (718.2): calcd. C 30.16, H 4.47, N 19.55; found C 30.39, H 4.77, N 19.73.

{[9](ClO₄)₂·4H₂O}: Yield 78 mg, 80%. M.p. > 350 °C. MS (ESI positive mode, MeOH/H_2O): *m*/*z* (%) = 893.2 (2) [M + H]$^+$, 793.2 (73) [M − ClO_4]$^+$, 731.4 (58) [M + 2 H − $ZnClO_4$]$^+$, 631.4 (50) [M + H − $ZnClO_4$ − ClO_4]$^+$, 569.5 (100) [M + 3 H − 2 $ZnClO_4$]$^+$. MS (FAB$^+$, 3-nitrobenzyl alcohol matrix): *m*/*z* (%) = 893.1 (23) [M + H]$^+$, 793.2 (63) [M$^+$ − ClO_4], 695 (100) [(M + H)$^+$ − 2 ClO_4], 731.3 (56) [M + H − $Zn(ClO_4)$]$^+$, 631.3 (77) [M + H − $Zn(ClO_4)_2$]$^+$. $C_{27}H_{46}N_{14}Zn_2(ClO_4)_2 \cdot 4H_2O$ (968.5): calcd. C 33.48, H 5.62, N 20.24; found C 33.26, H 5.40, N 20.46.

{[10](ClO₄)₂·6H₂O}: Yield 91 mg, 75%. M.p. > 350 °C. MS (ESI positive mode, MeOH/H_2O): *m*/*z* (%) = 995.1 (5) [(M − ClO_4]$^+$, 833.0 (31) [M + H − $Zn(ClO_4)_2$]$^+$, 733.5 (54) [M − Zn − 3 ClO_4]$^+$, 671.2 (100) [M + 2 H − 2 Zn − 3 ClO_4]$^+$, 571.6 (91) [M + H − 2 $Zn(ClO_4)_2$]$^+$. MS (FAB$^+$, 3-nitrobenzyl alcohol matrix): *m*/*z* (%) = 996.1 (20) [(M + H)$^+$ − ClO_4], 995.1 (44) [M$^+$ − ClO_4], 897 (33) [(M + 2 H)$^+$ − 2 ClO_4], 895 (21) [M$^+$ − 2 ClO_4], 733.3 (23) [M$^+$ − $Zn(ClO_4)_2$ − ClO_4], 633.3 (30) [M$^+$ − $Zn(ClO_4)_2$ − $HClO_4$]. $C_{32}H_{46}N_{10}Zn_2(ClO_4)_4 \cdot 6H_2O$ (1207.5): calcd. C 31.84, H 4.81, N 11.61; found C 31.91, H 5.17, N 11.69.

Synthesis of M^{II} Dinuclear Complexes from the Disodium Dipyrazolate Salt 4′

Preparation of $[Cu_2(H_{-2}L^4)](ClO_4)_2$ {[11]$(ClO_4)_2$}: To a stirred solution of the sodium dipyrazolate salt **4′** (53 mg, 0.1 mmol) in MeOH (2 mL) was added a solution of $Cu(ClO_4)_2·6H_2O$ (74 mg, 0.2 mmol) in 2 mL of the same solvent dropwise under argon. The mixture was stirred at room temperature overnight and the desired complex $[Cu_2(H_{-2}L^4)](ClO_4)_2$ {[**11**]$(ClO_4)_2$} separated as a blue precipitate. This was isolated by filtration, dried under vacuum and crystallised from a water/methanol mixture (2:3) (16 mg, 21%); m.p. > 350 °C. MS (ESI positive mode, H_2O/MeOH): *m/z* (%) = 671.0 (100) $[M - ClO_4]^+$, 571.2 (58) $[M - ClO_4 - HClO_4]^+$, 508.1 (9) $[M + H - Cu(ClO_4)_2]^+$. $C_{22}H_{40}Cu_2N_{10}(ClO_4)_2$ (770.61): calcd. C 34.28, H 5.23, N 18.17; found C 34.05, H 4.98, N 17.96.

Preparation of Zn^{II} Dinuclear Complex $[Zn_2(H_{-2}L^4)](ClO_4)_2$ {[12]$(ClO_4)_2$}: To a stirred solution of the sodium dipyrazolate salt of **4′** (53 mg, 0.1 mmol) in MeOH (2 mL) was added a solution of $Zn(ClO_4)_2·6H_2O$ (74 mg, 0.2 mmol) in 2 mL of the same solvent dropwise under argon. The mixture was stirred at room temperature overnight and the title complex precipitated. It was then isolated by filtration, dried under vacuum and crystallised from a water/methanol mixture (2:3) to afford $[Zn_2(H_{-2}L^4)](ClO_4)_2$ {[**12**]$(ClO_4)_2$} as a white solid (27 mg, 35%); m.p. > 350 °C. MS (ESI positive mode, H_2O/MeOH): *m/z* (%) = 671.2 (32) $[M - ClO_4]^+$, 609.3 (27) $[M + 2\,H - Zn - ClO_4]^+$, 575.2 (51) $[M + H - 2\,ClO_4H]^+$, 509.4 (100) $[M + H - Zn(ClO_4)_2]^+$, 447.4 (64) $[M + 3\,H - Zn(ClO_4)_2 - Zn]^+$. $C_{22}H_{40}N_{10}Zn_2(ClO_4)_2$ (774.3): calcd. C 34.13, H 5.21, N 18.09; found C 33.99, H 5.24, N 17.97.

Synthesis of Cu^{II} Dinuclear Complexes from Ligand 4

Preparation of Cu^{II} Dinuclear Complex $[Cu_2L^4](ClO_4)_4·2H_2O$ {[13]$(ClO_4)_4·2H_2O$} (Blue and Red Forms): Working under argon, a solution of $Cu(ClO_4)_2·6H_2O$ (74 mg, 0.2 mmol) in dry MeOH (2 mL) was added with stirring to a solution of the polyamine ligand **4** (45 mg, 0.1 mmol) in 2 mL of same solvent. After 4 h, a blue precipitate had formed. This was filtered off and vacuum-dried at 100 °C over phosphorus pentoxide for 24 h to give a blue solid (72 mg, 71%); m.p. > 350 °C. MS (ESI negative mode, H_2O/MeOH): *m/z* (%) = 1070.9 (35) $[M + ClO_4]^-$, 968.8 (6) $[M - H]^-$, 869.0 (100) $[M - (HClO_4 + H)]^-$. MS (ESI positive mode, H_2O/MeOH): *m/z* (%) = 871.0 (10) $[(M - ClO_4]^+$, 771.0 (10) $[(M - (HClO_4 + ClO_4)]^+$, 710.2 (30) $[M - Cu(ClO_4)_2 + H]^+$, 671.1 (100) $[M - (2\,HClO_4 + ClO_4)]^+$, 608.1 (5) $[M - \{Cu(ClO_4)_2 + ClO_4\}]^+$, 547.3 (51) $[M - \{Cu(ClO_4)_2 + CuClO_4\} + 2\,H]^+$. $C_{22}H_{40}Cu_2N_{10}(ClO_4)_2(HClO_4)_2(H_2O)_2$ (1007.56): calcd. C 26.23, H 4.60, N 13.90; found C 26.21, H 4.54, N 13.69. When the above blue solid was heated to reflux in water (5 mL) for 5 min and the resultant blue aqueous solution allowed to stand at room temperature, a red precipitate was unexpectedly obtained upon slow evaporation of the solvent. This was filtered off, washed with methanol and vacuum-dried at 100 °C over phosphorus pentoxide for 24 h to give the complex {red-[**13**]$(ClO_4)_4·2H_2O$} as a brown-reddish solid (61 mg, 60%); m.p. > 350 °C. MS (ESI negative mode, H_2O/MeOH): *m/z* (%) = 1071.4 (100) $[M + ClO_4]^-$, 969.4 (15) $[M - H]^-$, 869.4 (83) $[M - (HClO_4 + H)]^-$. MS (ESI positive mode, H_2O/MeOH): *m/z* (%) = 871.0 (3) $[M - ClO_4]^+$, 771.0 (4) $[M - (HClO_4 + ClO_4)]^+$, 710.1 (22) $[M - Cu(ClO_4)_2 + H]^+$, 671.1 (59) $[M - (2\,HClO_4 + ClO_4)]^+$, 608.1 (23) $[M - \{Cu(ClO_4)_2 - ClO_4\}]^+$, 547.3 (33) $[M - \{Cu(ClO_4)_2 + CuClO_4\} + 2\,H]^+$, 447.4 (41) $[M - 2\,Cu(ClO_4)_2 + H]^+$, 224.3 (100) $[\{M - 2\,Cu(ClO_4)_2\}/2 + H]^+$. MS ($FAB^+$, 3-nitrobenzyl alcohol matrix): *m/z* (%) = 871.1 (3) $[M - ClO_4]^+$, 771.2 (12) $[M - (HClO_4 + ClO_4)]^+$, 710.3 (7) $[M - Cu(ClO_4)_2 + H]^+$, 671.2 (100) $[M - (2\,HClO_4 + ClO_4)]^+$, 608.3 (5) $[M - \{Cu(ClO_4)_2 - ClO_4\}]^+$, 659.2 (44) $[M - \{3\,HClO_4 + ClO_4\}]^+$, 507.3 (7) $[M - \{Cu(ClO_4)_2 + 2\,HClO_4\}^{·+}]$. $C_{22}H_{42}Cu_2N_{10}(ClO_4)_4·2H_2O$ (1007.56): calcd. C 26.23, H 4.60, N 13.90; found C 26.31, H 4.77, N 13.86.

Preparation of the Green Cu^{II} Trinuclear Complex $[Cu_3(H_{-2}L^4)](ClO_4)_4·2MeOH$ {[14]$(ClO_4)_4·2MeOH$}: Basic anion-exchange resin (DOWEX, 550A OH) was added in portions to a stirred solution of [**4**]·6HCl (100 mg, 0.14 mmol) in H_2O (20 mL) until a pH of 11−12 was reached. The resin was then filtered off and the solvent removed under reduced pressure. The resultant solid was crystallised from toluene to give **4** as a white solid of m.p. 154−156 °C. Then, working under argon, a solution of $Cu(ClO_4)_2·6H_2O$ (93 mg, 0.24 mmol) in dry MeOH (1 mL) was added with stirring to a solution of the above polyamine $\mathbf{L^4}$ (**4**) (56 mg, 0.12 mmol) in 1 mL of the same solvent. After 4 h, a green precipitate was formed. This was filtered off and vacuum-dried at 100 °C over phosphorus pentoxide for 24 h to afford compound [**14**]$(ClO_4)_4·2MeOH$ as a green solid; m.p. > 350. MS (FAB^+, 3-nitrobenzyl alcohol matrix): *m/z* (%) = 927.7 (6) $[M - (2\,MeOH + ClO_4H + 4\,H)]^+$, 867.7 (14) $[M - (2\,Me + 2\,ClO_4)]^+$, 827.7 (80) $[M - (2\,MeOH + 2\,ClO_4H + 4\,H)]^+$, 732.1 (59) $[M - (2\,MeOH + 2\,ClO_4H + ClO_4)]^+$, 671.3 (51) $[M - \{2\,MeOH + Cu(ClO_4)_2 + ClO_4\}]^+$, 633.2 (100) $[M - (2\,MeOH + 2\,ClO_4H + ClO_4)]^+$, 569.3 (37) $[M - \{2\,MeOH + Cu(ClO_4)_2 + HClO_4H + ClO_4\}]^+$. MS (MALDI-TOF, 2,5-dihydroxybenzoic acid matrix): *m/z* (%) = 851.2 (16) $[(M - (Me + MeO + 2\,ClO_4)]^+$, 797.2 (27) $[M - 3\,ClO_4 + ClO_4H]^+$, 750.3 (7) $[M - (MeOH + Me + 3\,ClO_4)]^+$, 734.3 (78) $[M - (2\,MeOH + 3\,ClO_4)]^+$, 672.3 (69) $[M - \{2\,MeOH + Cu(ClO_4)_2 + ClO_4\}]^+$, 649.4 (26) $[M - (MeOH + Me + 4\,ClO_4)]^+$, 635.4 (100) $[M - 2\,MeOH + 4\,ClO_4]^+$. $C_{22}H_{40}Cu_3N_{10}(ClO_4)_4·2MeOH$ (1097.14): calcd. C 26.27, H 4.41, N 12.77; found C 26.06, H 4.08, N 12.38.

X-ray Crystallography: Crystal data and details of the data collection for the complexes $[Zn_2(H_{-2}\mathbf{L^1})](ClO_4)_2$ {[**8**]$(ClO_4)_2$}, $[Cu_2(H_{-2}L^4)](ClO_4)_2$ {[**11**]$(ClO_4)_2$} and $[Zn_2(H_{-2}L^4)](ClO_4)_2$ {[**12**]$(ClO_4)_2$} are given in Table 13. The crystal data were collected with a Nonius Kappa CCD instrument (λ = 0.71073 Å). In the case of [**11**]$(ClO_4)_2$ and [**12**]$(ClO_4)_2$ the data were collected at 120 K. The crystals were monitored for decay during data collection and appropriate corrections were made where necessary. A profile analysis was performed on every reflection.[37] A semiempirical absorption correction, Ψ-scan based, was performed in each case.[38] Lorentz and polarisation corrections were applied and the data were reduced to F_o^2 values. The structures were solved by Patterson methods using SHELXS-86 with an IBM PENTIUM II 300 computer.[39] Isotropic least-squares refinements were performed using SHELXL-93.[40] The hydrogen atoms were placed in calculated positions. All non-hydrogen atoms were refined anisotropically. The hydrogen atoms were refined with a common thermal parameter. Atomic scattering factors were taken from the International Tables for X-ray Crystallography.[41] The molecular plots were produced using ORTEP.[42] CCDC-240640, -240641 and -240642 contain the supplementary crystallographic data for structures [**8**]$(ClO_4)_2$, [**11**]$(ClO_4)_2$ and [**12**]$(ClO_4)_2$, respectively. These data can be obtained free of charge via www.ccdc.cam.ac.uk/const/retrieving.html [or from the Cambridge Crystallographic Data Centre, 12 Union Road, Cambridge CB2 1EZ, UK; Fax: (internat.) + 44-1223-336-033; or E-mail: deposit@ccdc.cam.ac.uk].

Electromotive Force (emf) Measurements: The potentiometric titrations were carried out in 0.15 M NaCl at 298.1 ± 0.1 K using the experimental procedure (burette, potentiometer, cell, stirrer,

Table 13. Crystallographic data for [**8**]$(ClO_4)_2$, [**11**]$(ClO_4)_2$ and [**12**]$(ClO_4)_2$

	[**8**]$(ClO_4)_2$	[**11**]$(ClO_4)_2$	[**12**]$(ClO_4)_2$
Empirical formula	$C_{19}H_{26}N_6O_8CL^2Zn_2$	$C_{21}H_{36}N_{10}O_8CL^2Cu_2$	$C_{21}H_{36}N_{10}O_8CL^2Zn_2$
M	668.1706	754.5724	758.2984
T [K]	293	293	293
Crystal system	triclinic	orthorhombic	orthorhombic
Colour	colourless	blue	colourless
Space group	$P\bar{1}$	*Pmcn*	*Pmcn*
a [Å]	10.4570(2)	13.762(1)	13.5330(7)
b [Å]	11.7980(2)	15.393(1)	15.3960(8)
c [Å]	13.3670(4)	15.524(2)	16.098(1)
α [°]	111.624(1)	90	90
β [°]	107.061(1)	90	90
γ [°]	100.304(2)	90	90
V [Å^3]	1387.06(5)	3288.6(5)	3354.1(3)
Z	2	4	4
$D_{calcd.}$ [g·cm^{-3}]	1.60	1.524	1.502
λ [Å]	0.7103	0.7103	0.7103
μ [mm^{-1}]	1.974	1.513	1.645
$F(000)$	680	1552	1560
θ range of data collection [°]	$1.83 < \theta < 27.39$	$1.86 < \theta < 21.76$	$1.83 < \theta < 27.39$
Index ranges	$-13 < h < 12$	$-13 < h < 13$	$-17 < h < 17$
	$-15 < k < 14$	$-16 < k < 16$	$-19 < k < 18$
	$0 < l < 17$	$-16 < l < 16$	$-19 < l < 20$
Number of reflections measured	6230	13525	5893
Unique reflections	630	2031	3348
Number of reflections observed [$I > 2\sigma(I)$]	3995	1133	1424
Parameters/restraints	393/0	245/0	261/0
Goodness of fit/Goof	1.051	0.944	1.049
R factor all reflections ωR_2	0.135	0.151	0.2087
R factor ωR_1	0.055	0.078	0.080
Max./min. nonassigned density [e/Å^3]	1.645/−0.742	0.919/−0.678	1.76/−1.49

Weighting details: $\omega = 1/[\sigma^2(F_o^2) + (0.1000P)^2 + 0.0000P]$ where $P = (F_o^2 + 2F_c^2)^{1/3}$

microcomputer, etc.) fully described elsewhere.[43] The acquisition of the emf data was performed with the computer program PASAT.[44] The reference electrode was an Ag/AgCl electrode in a saturated KCl solution. The glass electrode was calibrated as a hydrogen ion concentration probe by titration of known amounts of HCl with CO_2-free NaOH solutions[45] and determination of the equivalent point by Gran's method[46] which gives the standard potential $E^{\circ\prime}$ and the ionic product of water [pK_w = 13.73(1)]. The computer program HYPERQUAD[47] was used to calculate the protonation and stability constants and the DISPO[48] program was used to obtain the distribution diagrams. The titration curves for each system (ca. 200 experimental points corresponding to at least three measurements, pH = 2−11, concentration of ligands 1×10^{-3} to 5×10^{-3} M) were treated either as a single set or as separated curves without significant variations in the values of the stability constants. Finally, the sets of data were merged and treated simultaneously to give the final stability constants.

Magnetic Measurements: Magnetic susceptibility measurements of polycrystalline samples were measured over the temperature range 2−300 K with a Quantum Design SQUID magnetometer using an applied magnetic field of 1 T. Diamagnetic corrections of the constituents atoms were estimated from Pascal's constants and a value of 60×10^{-6} cm^3·mol^{-1} was used for the temperature-independent paramagnetism of each copper(II) ion.

Paramagnetic ^{1}H NMR Spectroscopy: Paramagnetic ^{1}H NMR spectra were recorded with a Varian Unity 400 spectrometer operating at 400 MHz. 1D spectra were recorded in $(CD_3)_2SO$ with presaturation of the $(CH_3)_2SO$ signal during part of the relaxation delay. Because the relaxation times were diverse, a variety of NMR parameters were utilised. Acquisition times from 40 to 80 ms, relaxation delay times from 50 to 200 ms, presaturation times from 50 to 200 ms, spectral widths of 40 to 100 kHz and 256 to 1024 of scans were used. 1D spectra were processed using exponential line-broadening weighting functions as apodisation with values of 20−40 Hz. Chemical shifts were referenced to the residual solvent protons of $(CD_3)_2SO$ resonating at δ = 2.50 ppm relative to $SiMe_4$. ^{1}H longitudinal relaxation times were calculated using the inversion recovery pulse sequence[49] (d_1 − 180° − τ − 90° − acq), 18 values of τ were selected, (d_1 + acq) values were 200 ms and the number of scans was 512. The T_1 values were calculated from the inversion-recovery equation. Transversal relaxation times were obtained by measuring the line broadening of the isotropically shifted signals at half-height with the equation $T_2^{-1} = \pi \Delta\nu_{1/2}$.

Molecular Modelling: Molecular modelling studies were carried out using the AMBER method implemented in the Hyperchem 6.0 package[50] and modified by the inclusion of appropriate parameters. Where available, the parameters were analogous to those reported in the literature.[29,50] All others, namely those regarding the particular atomic connections of our ligands with the metal ion, were developed according to the Norrby procedures[28,51] in a similar way to the ones used in the MOMEC program.[52] The equilibrium bond lengths and angles were derived from experimental values on reasonable reference compounds. All additional parameters are given in the Supporting Information (Table S1). The starting structures were built using Hyperchem capabilities and geometries were minimised to a maximum energy gradient of 0.1 kcal/(Å mol) using the Polak−Ribiere (conjugate gradient) algorithm.

Supporting Information: Table S1 includes nonstandard force field parameters used in the modelling. Figures S1 (A−C) show the ^1H NMR spectra of **L⁴** at pH values 10.5, 8 and 3.7. Figure S2 represents χ_M vs. T for compounds red-[**13**]$(ClO_4)_4 \cdot 2H_2O$ and [**11**]$(ClO_4)_2$.

Acknowledgments

Financial support by the Spanish "Comisión Interministerial de Ciencia y Tecnología" (CICYT, SAF-99-0063 and BQU2003-09215-CO3-01) and Generalitat Valenciana (CTIDIB/2002/244 and Grupos03/196) is gratefully acknowledged.

[1] [1a] W. Kaim, B. Schwederski, *Bioinorganic Chemistry: Inorganic Elements in the Chemistry of Life, An Introduction and Guide*, John Wiley & Sons, Chichester, **1995**. [1b]R. H. Holm, E. I. Solomon, *Chem. Rev.* **1996**, *96*, 2237−3042. [1c] I. Bertini, H. B. Gray, S. J. Lippard, J. S. Valentine, *Bioinorganic Chemistry*, University Science Books, Mill Valley, California, **1994**.

[2] [2a] J. P. Collman, *Acc. Chem. Res.* **1977**, *10*, 265−272. [2b] G. Feher, J. P. Allen, M. Y. Okamura, D. C. Rees, *Nature (London)* **1989**, *339*, 111−116. [2c] N. Kitajima, Y. Moro-oka, *J. Chem. Soc., Dalton Trans.* **1993**, 2665−2671. [2d] P. Woolley, *Nature (London)* **1975**, *258*, 677−682. [2e] S. H. Gellman, R. Petter, R. Breslow, *J. Am. Chem. Soc.* **1986**, *108*, 2388−2394. [2f] T. Koike, S. Kajitani, I. Nakamura, E. Kimura, M. Shiro, *J. Am. Chem. Soc.* **1995**, *117*, 1210−1219. [2g] R. Breslow, *Acc. Chem. Res.* **1995**, *28*, 146−153.

[3] [3a] R. H. Holm, E. I. Solomon, *Chem. Rev.* **1996**, *96*, 2237−3042. [3b] B. A. Mackay, M. D. Fryzuk, *Chem. Rev.* **2004**, *104*, 385−401. [3c] T. Nakamura, Y. Yammamoto, *Chem. Rev.* **2004**, *104*, 2127−2198.

[4] [4a] B. Rosenberg, L. Van Camp, K. Trigas, *Nature (London)* **1965**, *205*, 698−699. [4b] B. Rosenberg, L. Van Camp, J. E. Trosko, V. H. Mansour, *Nature (London)* **1969**, *222*, 385−386. [4c] C. Orvig, M. J. Abrams, *Chem. Rev.* **1999**, *99*, 2201−2842.

[5] [5a] D. Parker, *Chem. Soc. Rev.* **1990**, *19*, 271−291. [5b] M. J. Abrahams, B. A. Murrer, *Science* **1993**, *261*, 725−730. [5c] S. Jurisson, D. Berning, W. Jia, D. Ma, *Chem. Rev.* **1993**, *93*, 1137−1156. [5d] M. J. Heeg, S. S. Jurisson, *Acc. Chem. Res.* **1999**, *32*, 1053−1060. [5e] S. Kobayashi, H. Uyama, S. Kimura, *Chem. Rev.* **2001**, *101*, 398−3818.

[6] X. Huang, M. P. Cuajungco, C. S. Atwood, M. A. Hartshorn, J. D. A. Tyndall, G. R. Hanson, K. C. Stokes, M. Leopold, G. Multhaup, L. E. Goldstein, R. C. Scarpa, A. J. Saunders, J. Lim, R. D. Moir, C. Glabe, E. F. Bowden, C. L. Masters, D. P. Fairlie, R. E. Tanzi, A. I. Bush, *J. Biol. Chem.* **1999**, *274*, 37111−37116.

[7] J. Elguero, "Pyrazoles" in *Comprehensive Heterocyclic Chemistry II, A Review of the Literature 1982−1995* (Eds.: A. R. Katritzky, C. V. Rees, E. F. V. Scriven), Elsevier Science Ltd., Oxford, **1996**, vol. 3.

[8] R. Mukherjee, *Coord. Chem. Rev.* **2000**, *203*, 151−218.

[9] V. J. Arán, M. Kumar, J. Molina, L. Lamarque, P. Navarro, E. García-España, J. A. Ramirez, S. V. Luis, B. Escuder, *J. Org. Chem.* **1999**, *64*, 6135−6146.

[10] L. Lamarque, C. Miranda, P. Navarro, F. Escartí, E. García-España, J. Latorre, J. A. Ramirez, *Chem. Commun.* **2000**, 1337−1338.

[11] L. Lamarque, P. Navarro, C. Miranda, V. J. Arán, C. Ochoa, F. Escartí, E. García-España, J. Latorre, S. V. Luis, J. F. Miravet, *J. Am. Chem. Soc.* **2001**, *123*, 10560−10570.

[12] [12a] A. Andrés, M. I. Burguete, E. García-España, S. V. Luis, J. F. Miravet, C. Soriano, *J. Chem. Soc., Perkin Trans. 2* **1993**, 749−755. [12b] A. Bianchi, B. Escuder, E. García-España, S. V. Luis, V. Marcelino, J. F. Miravet, J. A. Ramírez, *J. Chem. Soc., Perkin Trans. 2* **1994**, 1253−1259. [12c] A. Andrés, C. Bazzicaluppi, A. Bianchi, E. García-España, S. V. Luis, J. F. Miravet, J. A. Ramírez, *J. Chem. Soc., Dalton Trans.* **1994**, 2995−3004.

[13] J. A. Aguilar, E. García-España, J. A. Guerrero, J. M. Llinares, J. A. Ramírez, C. Soriano, S. V. Luis, A. Bianchi, L. Ferrini, V. Fusi, *J. Chem. Soc., Dalton Trans.* **1996**, 239−246.

[14] A. Bencini, A. Bianchi, E. García-España, M. Micheloni, J. A. Ramírez, *Coord. Chem. Rev.* **1999**, *188*, 97−156.

[15] L. Behle, M. Neuburger, M. Zehnder, T. A. Kaden, *Helv. Chim. Acta* **1995**, *78*, 693−702.

[16] H. Weller, L. Siegfried, M. Neuburger, M. Zehnder, T. A. Kaden, *Helv. Chim. Acta* **1997**, *80*, 2315−2328.

[17] M. Kumar, V. J. Arán, P. Navarro, A. Ramos-Gallardo, A. Vegas, *Tetrahedron Lett.* **1994**, *35*, 5723−5726.

[18] M. Kumar, V. J. Arán, P. Navarro, *Tetrahedron Lett.* **1993**, *34*, 3159−3162.

[19] M. Kumar, V. J. Arán, P. Navarro, *Tetrahedron Lett.* **1995**, *36*, 2161−2164.

[20] [20a] S. F. Ralph, M. M. Sheil, L. A. Hick, R. J. Geue, A. M. Sargeson, *J. Chem. Soc., Dalton Trans.* **1996**, 4417−4424. [20b] A. Matsumoto, T. Fukumoto, H. Adachi, H. Watarai, *Anal. Chim. Acta* **1999**, *390*, 193−199 and references contained therein. [20c] N. Yoshida, K. Ichikawaa, M. Shirob, *J. Chem. Soc., Perkin Trans. 2* **2000**, 17−26.

[21] E. L. Muetterties, L. J. Guggenberger, *J. Am. Chem. Soc.* **1974**, *96*, 1748−1756.

[22] [22a] J. Ackermann, F. Meyer, E. Kaifer, H. Pritzkow, *Chem. Eur. J.* **2002**, *8*, 247−258. [22b] F. Meyer, A. Jacobi, B. Nuber, P. Rutsch, L. Zsolnai, *Inorg. Chem.* **1998**, *37*, 1213−1218.

[23] R. Zenobi, R. Knochenmuss, *Mass Spectrom. Rev.* **1998**, *17*, 337−366.

[24] [24a] E. Lehmann, R. Knochenmuss, R. Zenobi, *Rapid Commun. Mass Spectrom.* **1997**, *11*, 1483−1492. [24b] R. Zenobi, *Chimia* **1997**, *51*, 801−803.

[25] P. Siemsen, U. Gubler, C. Bosshard, P. Guenter, F. Diederich, *Chem. Eur. J.* **2001**, *7*, 1333−1341.

[26] [26a] P. Comba, T. W. Hambley, *Molecular Modelling of Inorganic Compounds*, VCH Publishers, New Cork, **1995**. [26b] C. R. Landis, D. M. Root, T. Cleveland, *Reviews in Computational Chemistry* (Eds.: K. B. Lipkowitz, D. B. Boyd), VCH Publishers, New York, **1995**, vol. 6, pp. 73−148. [26c] M. Zimmer, *Chem. Rev.* **1995**, *95*, 2629−2649.

[27] W. D. Cornell, P. Cieplak, C. I. Bayly, I. R. Gould, K. M. J. Merz, D. M. Ferguson, D. C. Spelmeyer, T. Fox, J. W. Caldwell, P. A. Kollman, *J. Am. Chem. Soc.* **1995**, *117*, 5179−5197.

[28] D. E. Reichert, P.-O. Norrby, M. J. Welch, *Inorg. Chem.* **2001**, *40*, 5223−5230.

[29] P. Comba, R. Remenyi, *Coord. Chem. Rev.* **2003**, *238−239*, 9−20.

[30] I. Bertini, C. Luchinat, "NMR of paramagnetic substances", in *Coord. Chem. Rev.* **1996**, *150*.

[31] N. N. Murthy, K. D. Karlin, I. Bertini, C. Luchinat, *J. Am. Chem. Soc.* **1997**, *119*, 2156−2162.

[32] [32a] F. Meyer, S. Beyreuther, K. Heinze, L. Zsolnai, *Chem. Ber./Recl.* **1997**, *130*, 605−614. [32b] F. Meyer, A. Jacobi, L. Zsolnai, *Chem. Ber./Recl.* **1997**, *130*, 1441−1448.

[33] [33a] T. Kamiusuki, H. Okawa, N. Matsumoto, S. Kida, *J. Chem. Soc., Dalton Trans.* **1990**, 195−198. [33b] V. P. Hanot, T. D. Robert, J. Kolnaar, J. G. Haasnoot, J. Reedijk, H. Kooijman, A. L. Spek, *J. Chem. Soc., Dalton Trans.* **1996**, 4275−4281. [33c] J. Pons, X. López, J. Casabo, F. Teixidor, A. Caubet, J. Rius, C. Miravitlles, *Inorg. Chim. Acta* **1992**, *195*, 61−66. [33d] R. Gupta, R. Hotchandani, R. Mukherjee, *Polyhedron* **2000**, *19*, 1429−1435. [33e] A. M. Schuitema, M. Engelen, I. A. Koval, S. Gorter, W. L. Driessen, J. Reedijk, *Inorg. Chim. Acta* **2001**, *324*, 57−64.

[34] P. Román, C. Guzmán-Miralles, A. Luque, J. I. Beitia, J. Cano, F. Lloret, M. Julve, S. Alvarez, *Inorg. Chem.* **1996**, *35*, 3741−3751.

[35] D. D. Perrin, W. L. F. Armarego, D. R. Perrin, *Purification of Laboratory Chemicals*, Pergamon Press, Oxford, **1980**.

[36] A. K. Covington, M. Paabo, R. A. Robinson, R. G. Bates, *Anal. Chem.* **1968**, *40*, 700−706.
[37] [37a] M. S. Lehmann, F. K. Larsen, *Acta Crystallogr., Sect. A* **1978**, *30*, 580−584. [37b] D. F. Grant, E. J. Gabe, *J. Appl. Crystallogr.* **1978**, *11*, 114−120.
[38] A. C. T. Nort, D. C. Phillips, F. S. Mathews, *Acta Crystallogr., Sect. A* **1968**, *24*, 351−359.
[39] G. M. Sheldrick, C. Kruger, R. Goddard, Editors, *Crystallographic Computing*, Clarendon Press, Oxford, England, **1985**, p. 175.
[40] G. M. Sheldrick, *SHELXL-93: Program for Crystal Structure Refinement*, Institut für Anorganische Chemie, University of Göttingen, Germany, **1993**.
[41] *International Tables for X-ray Crystallography*, The Kynoch Press: Birmingham, England, **1974**, vol. IV.
[42] C. K. Johnson, ORTEP; Report ORNL-3794, Oak Ridge National Laboratory, Oak Ridge, TN, **1971**.
[43] E. García-España, M.-J. Ballester, F. Lloret, J. M. Moratal, J. Faus, A. Bianchi, *J. Chem. Soc., Dalton Trans.* **1988**, 101−104.
[44] M. Fontanelli, M. Micheloni, *Proc. 1st Spanish-Italian Congr. Thermodynamics of Metal Complexes*, Peñíscola, Castellón (Spain), June 3−6, **1990**.
[45] M. Micheloni, A. Sabatini, A. Vacca, *Inorg. Chim. Acta* **1977**, *25*, 41.
[46] [46a] G. Gran, *Analyst (London)* **1952**, *77*, 661−671. [46b] F. J. C. Rossoti, H. Rossoti, *J. Chem. Educ.* **1965**, *42*, 375−378.
[47] P. Gans, A. Sabatini, A. Vacca, *Talanta* **1996**, *43*, 1739−1753.
[48] A. Vacca, *FORTRAN program for the determination of species distribution in multicomponent systems*, Florence, **1977**.
[49] A. E. Derome, *Modern NMR Techniques for Chemistry Research*, Pergamon Press, Oxford, **1987**.
[50] Hyperchem 6.0 (Hypercube Inc), Scientific Software, USA, **2000**.
[51] [51a] P. V. Bernhardt, P. Comba, *Inorg. Chem.* **1992**, *31*, 2638−2644. [51b] J. E. Bol, C. Buning, P. Comba, J. Reedijk, M. Ströhle, *J. Comput. Chem.* **1998**, *19*, 512−523. [51c] P.-O. Norrby, P. Brandt, *Coord. Chem. Rev.* **2001**, *212*, 79−109. [51d] C. Miranda, F. Escartí, L. Lamarque, M. J. R. Yunta, P. Navarro, E. García-España, M. L. Jimeno, *J. Am. Chem. Soc.* **2004**, *126*, 823−833.
[52] T. W. Hambley, G. Laur, N Okon, *MOMEC 97*, Heidelberg, Germany, **1997**.

Received August 2, 2004
Early View Article
Published Online November 18, 2004